ARTICLE



Genome-wide screening identifies novel genes implicated in cellular sensitivity to BRAF^{V600E} expression

Tengyu Ko¹ · Rahul Sharma^{2,3} · Shisheng Li¹

Received: 20 December 2018 / Revised: 10 September 2019 / Accepted: 11 September 2019 / Published online: 23 September 2019 © The Author(s), under exclusive licence to Springer Nature Limited 2019

Abstract

The V600E mutation of BRAF (BRAF^{V600E}), which constitutively activates the ERK/MAPK signaling pathway, is frequently found in melanoma and other cancers. Like most other oncogenes, BRAF^{V600E} causes oncogenic stress to normal cells, leading to growth arrest (senescence) or apoptosis. Through genome-wide screening, we identified genes implicated in sensitivity of human skin melanocytes and fibroblasts to BRAF^{V600E} overexpression. Among the identified genes shared by the two cell types are proto-oncogenes ERK2, a component of the ERK/MAPK pathway, and VAV1, a guanine nucleotide exchange factor for Rho family GTPases that also activates the ERK/MAPK pathway. CDKN1A, which has been known to promote senescence of fibroblasts but not melanocytes, is implicated in sensitivity of the fibroblasts but not the melanocytes to BRAF^{V600E} overexpression. Disruptions of GPR4, a pH-sensing G-protein coupled receptor, and DBT, a subunit of the branched chain α -keto acid dehydrogenase that is required for the second and rate-limiting step of branched amino acid catabolism and implicated in maple syrup urine disease, are the most highly selected in the melanocytes upon BRAF^{V600E} overexpression. Disruption of DBT severely attenuates ERK/MAPK signaling, p53 activation, and apoptosis in melanocytes, at least in part due to accumulation of branched chain α -keto acids. The expression level of BRAF positively correlates with that of DBT in all cancer types and with that of GPR4 in most cancer types. Overexpression of DBT kills all four melanoma cell lines tested regardless of the presence of BRAF^{V600E} mutation. Our findings shed new lights on regulations of oncogenic stress signaling and may be informative for development of novel cancer treatment strategies.

Introduction

Activation of oncogenes as a consequence of mutation or overexpression is a tumor-promoting event and a necessary step in tumorigenesis in many cancer types [1]. However, the initial promotion of proliferation by activated oncogenes

Supplementary information The online version of this article (https://doi.org/10.1038/s41388-019-1022-0) contains supplementary material, which is available to authorized users.

- Shisheng Li shli@lsu.edu
- Department of Comparative Biomedical Sciences, School of Veterinary Medicine, Louisiana State University, Baton Rouge, LA 70803, USA
- National Hansen's Disease Program, Laboratory Research Branch at Louisiana State University, 3519E School of Veterinary Medicine, Baton Rouge, LA 70803, USA
- ³ Present address: NuProbe Inc, Cambridge, MA 02140, USA

causes cellular stresses, which most often leads to cell senescence, an irreversible cell cycle arrest, or apoptosis [2–7]. The so-called oncogene-induced senescence and apoptosis serve as fail-safe mechanisms for suppressing tumorigenesis by preventing proliferation of cells at risk for neoplastic transformation. Whether a stressed cell commits senescence or apoptosis appears to be determined by the stress level and the balance between prosenescence and proapoptosis signaling pathways in the cell [7, 8]. In certain circumstances, overwhelming stresses result in apoptosis, whereas less severe stresses cause senescence. The p53-p21 and p16INK4a-Rb signaling pathways are known to be important for cellular response to stresses, including oncogenic stresses [3, 8, 9]. To date, however, how the oncogenic stress signaling pathways are regulated is still not well understood.

The proto-oncogene BRAF is a serine/threonine protein kinase that transduces signals downstream of RAS via the ERK/MAPK pathway [10]. BRAF is one of the most commonly mutated oncogenes in human cancers, including melanoma (40–50%), thyroid cancers (10–70%, depending

on the histological classification), colorectal cancers $(\sim 10\%)$, and nonsmall cell lung cancer (3-5%) [11]. Approximately 80% of activating BRAF mutations is glutamic acid substitution of valine at position 600 (BRAF^{V600E}) [12]. BRAF^{V600E} has a high protein kinase activity and is constitutively active, which is believed to contribute to the constant proliferation of melanoma cells [13]. However, BRAF^{V600E} alone appears to be insufficient for melanomagenesis, because the mutation is also highly (~82%) present in the precancerous skin melanocytic nevi, which are growth arrested and display classical hallmarks of cellular senescence [14, 15]. BRAF^{V600E} expression in cultured human primary melanocytes has been shown to induce senescence [14]. IL-6 and CXCR2 (also called IL-8 receptor type 2), which modulate cell proliferation and/or migration via autocrine or paracrine signaling, have been demonstrated to be required for BRAFV600E induced senescence [16, 17]. Activation of PI3K signaling has also been shown to abrogate BRAFV600E-induced senescence [18]. However, the mechanisms of BRAF^{V600E}-induced senescence appear to be multifaceted and, to date, the spectrum of genes implicated in the processes remains largely unknown. Also, although senescence and apoptosis appear to be two parallel fail-safe mechanisms for suppressing tumorigenesis, little has been known about how apoptosis is regulated to suppress melanomagenesis upon BRAF^{V600E} expression. This may be due to the fact that primary melanocytes, which typically commit senescence rather than apoptosis upon BRAF^{V600E} expression, have been used for most of the related studies.

By utilizing the CRISPR/Cas9 technology, we performed genome-wide screening of genes implicated in sensitivity of human melanocytes and fibroblasts to BRAF^{V600E} over-expression. A large fraction of the identified genes are shared by the melanocytes and fibroblasts, while some appear to be specific to the different cell types. In addition to several proto-oncogenes and tumor suppressor genes, we identified genes that have not been previously recognized as being implicated in oncogenic stresses.

Results

Genome-wide CRISPR/Cas9 knockout screening of genes implicated in sensitivity to BRAF^{V600E} overexpression

It has been largely unknown about the genes implicated in regulation of apoptosis upon BRAF^{V600E} expression. To identify these genes, it would be ideal to overexpress BRAF^{V600E} in cells with intact apoptosis but impaired senescence response. We therefore tested the human Hermes 4C skin melanocytes, which were immortalized by expressing

both human telomerase (TERT) and protein E7 from human papillomavirus type 16 (HPV16-E7) [19, 20]. HPV16-E7 binds to and impairs the functions of the retinoblastoma protein Rb, which is essential for cellular senescence [21, 22]. We transduced the Hermes 4C melanocytes with a lentiviral vector cocistronically expressing human BRAF v600E and GFP under the strong EF1 α (EF-BRAF^{V600E}-GFP) or the moderate PGK (PGK–BRAF^{V600E}–GFP) promoter (Fig. 1a). As a control, we also transduced the cells with a lentiviral vector expressing GFP under the EF1α promoter (EF–GFP) (Fig. 1a). The level of total BRAF expression in the cells transduced with EF-BRAF^{V600E}-GFP was ~2 times that transduced with PGK-BRAF V600E-GFP and 5-10 times those in the melanoma cell lines tested (Fig. 1b). Transduction with the EF-BRAF^{V600E}-GFP, and to a lesser extent with the PGK-BRAF^{V600E}-GFP, caused killing of the melanocytes, as evidenced by cell detachment from the surface of the culturing containers (Fig. 1, compare E with C and D). The killing was due to apoptosis as evidenced by Annexin V staining (Fig. 1f). Transduction with EF-GFP caused little, if any, killing of the melanocytes (Fig. 1d and data not shown). A small fraction of the EF-BRAF^{V600E}-GFP or PGK-BRAF^{V600E}-GFP transduced cells became enlarged to a certain extent and showed increased levels of senescenceassociated β-galactosidase (SA-β-gal) activity (Fig. 1, compare G and H), reflecting cellular senescence [23]. However, all the enlarged, high SA-β-gal-containing cells died out within 2 weeks of culture. This indicates that expression of HPV16-E7 in human melanocytes may indeed tilt the cellular response to BRAFV600E overexpression toward apoptosis over senescence.

Had established that the Hermes 4C melanocytes are responsive to BRAF^{V600E} overexpression-induced apoptosis (and to a much lesser extent, senescence), we wished to identify the genes implicated in the process. We transduced the cells with the human genome-scale CRISPR knockout (GeCKO, v2) lentiviral pooled libraries (Supplementary Table S1), which encode $\sim 1.2 \times 10^5$ unique single-guide RNAs (sgRNAs) targeting 99.4% of all human genes (six sgRNAs per gene and up to four sgRNAs per miRNA) [24]. One week after the transduction (when the majority of the GeCKO libraries-mediated gene disruption events had occurred), the cells were pooled and half of them were saved as control and the other half further transduced with the EF-BRAF^{V600E}-GFP (Fig. 1a). The fraction of GFPpositive cells was ~95% 4 days after the BRAF^{V600E}–GFP transduction (Fig. 2a), but diminished to ~1.7% 14 days after the transduction (Fig. 2b), indicating that only a small fraction of the cells could tolerate the BRAFV600E overexpression. The cells (14 day after EF-BRAF^{V600E}-GFP transduction) were sorted by using fluorescence-activated cell sorting (FACS), which enriched the GFP-positive cells to ~80%. A fraction of these cells endured prolonged

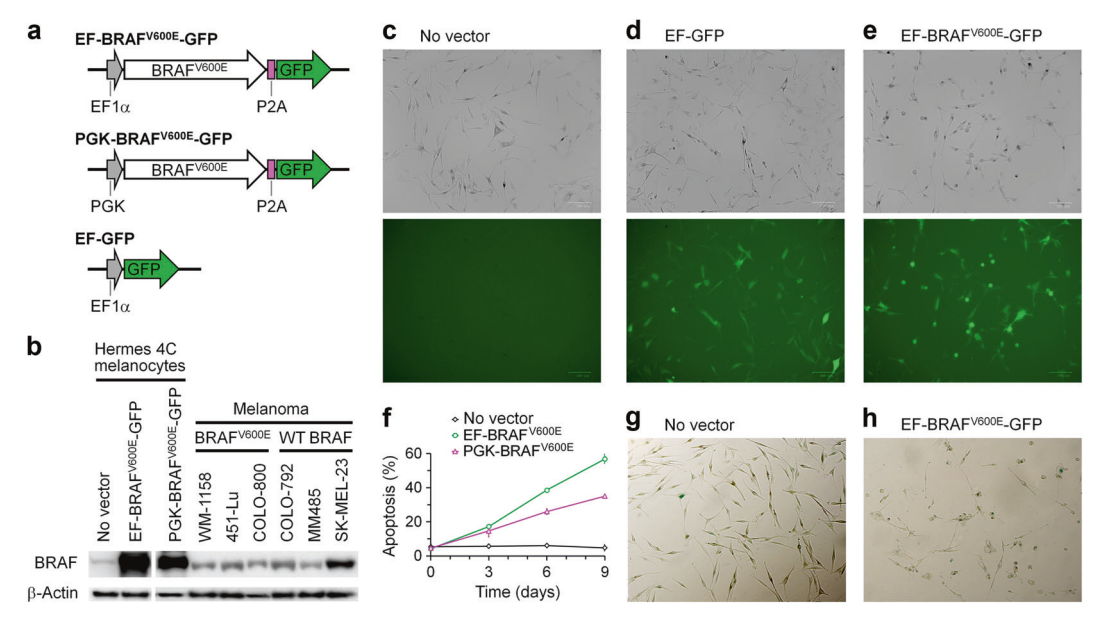


Fig. 1 BRAF^{V600E} overexpression in Hermes 4C human melanocytes primarily induces apoptosis. **a** Structures of lentiviral vectors EF-BRAF^{V600E}-GFP, PGK-BRAF^{V600E}-GFP and EF-GFP. **b** Western blot showing expression of the total BRAF protein in Hermes 4C melanocytes without vectors or 4 days after transduction with EF-BRAF^{V600E}-GFP and PGK-BRAF^{V600E}-GFP, and in selected melanoma cell lines (without vectors). **c-e** Bright-field (top) and fluorescence (bottom) microscopy images of Hermes 4C melanocytes

without vector (**c**) or 6 days after EF–GFP (**d**) or EF–BRAF^{V600E}–GFP (**e**) transduction. **f** Apoptosis of Hermes 4C melanocytes without vector or at different times after EF–BRAF^{V600E}–Hyg and PGK–BRAF^{V600E}–Hyg transduction. The cells were stained with Fluorescein-conjugated Annexin V. Error bars stand for standard errors. **g**, **h** Microscopy images of Hermes 4C melanocytes stained with *senescence-associated* β -galactosidase reagents without vector or 6 days after EF–BRAF^{V600E}–GFP transduction

culture, although the fraction of the GFP-positive cells continued to drop to a certain extent (Fig. 2c). However, if the cells were not transduced with the GeCKO libraries in advance, no GFP-positive cells can be detected 2 weeks after the EF-BRAF^{V600E}-GFP transduction. This indicates that disruption of certain gene(s) by the GeCKO libraries enabled a small fraction of the melanocytes to tolerate the BRAF^{V600E} overexpression.

We also performed the same GeCKO screening in the P1F/TERT human skin fibroblasts, which were immortalized by expressing human TERT. One week after transduction with the GeCKO libraries, the P1F/TERT cells were further transduced with the EF-BRAF^{V600E}-GFP (Fig. 1a). The fraction of GFP-positive cells dropped dramatically during the period of posttransduction culturing, although the dropping speed appeared to be slower than that of the Hermes 4C melanocytes (Fig. 2, compare panels D and E with A and B). Like the situation with the Hermes 4C melanocytes, only a small fraction of the GFP-positive fibroblasts appeared to be able to endure prolonged culture.

To identify the genes whose disruption might have enabled survival of the cells overexpressing BRAF^{V600E}, we analyzed the sgRNAs presented in these cells. The GFP-positive Hermes 4C melanocytes and P1F/TERT fibroblasts were collected by using FACS 52 and 91 days after the EF-BRAF^{V600E}-GFP transduction, respectively (Fig. 2f, g).

Total genomic DNA was isolated from the control (which were transduced with the GeCKO libraries but not the EF-BRAF^{V600E}-GFP) and the survived GFP-positive cells collected by FACS. The sgRNA-encoding sequences in the GeCKO libraries that had integrated in the genomic DNA were identified by next-generation sequencing and analyzed by using MAGeCK-VISPR, which assesses positively and negatively selected genes by testing whether their targeting sgRNA abundancies differ significantly between control and treated samples [24, 25]. Most of our sequencing reads are of high quality (Phred quality score ≥ 35) (Fig. 2h). Over 3 million reads from the controls of melanocytes (Mel_-Control) and fibroblast (Fib_Control) were perfectly mapped to the GeCKO sgRNAs (Fig. 2i) with reasonably good distribution and coverage (<800 out of the 1.2×10^5 sgRNAs were missing in the controls) (Fig. 2j–1). However, only 90 and 187 sgRNAs were detected in the BRAF^{V600E}-(GFP-positive) melanocytes overexpressing BRAF^{V600E}) and fibroblasts (Fib_BRAF^{V600E}), respectively (Supplementary Tables S2 and S3). This indicates that disruption of only a small number of genes by the GeCKO libraries may enable the melanocytes or fibroblasts to tolerate the BRAF^{V600E} overexpression.

Among the 90 sgRNAs (respectively targeting 90 different genes) detected in the BRAF^{V600E}-overexpressing Hermes 4C melanocytes, 26 were significantly enriched [p value < 1×10^{-6} and false discovery rate (FDR) < 0.1]

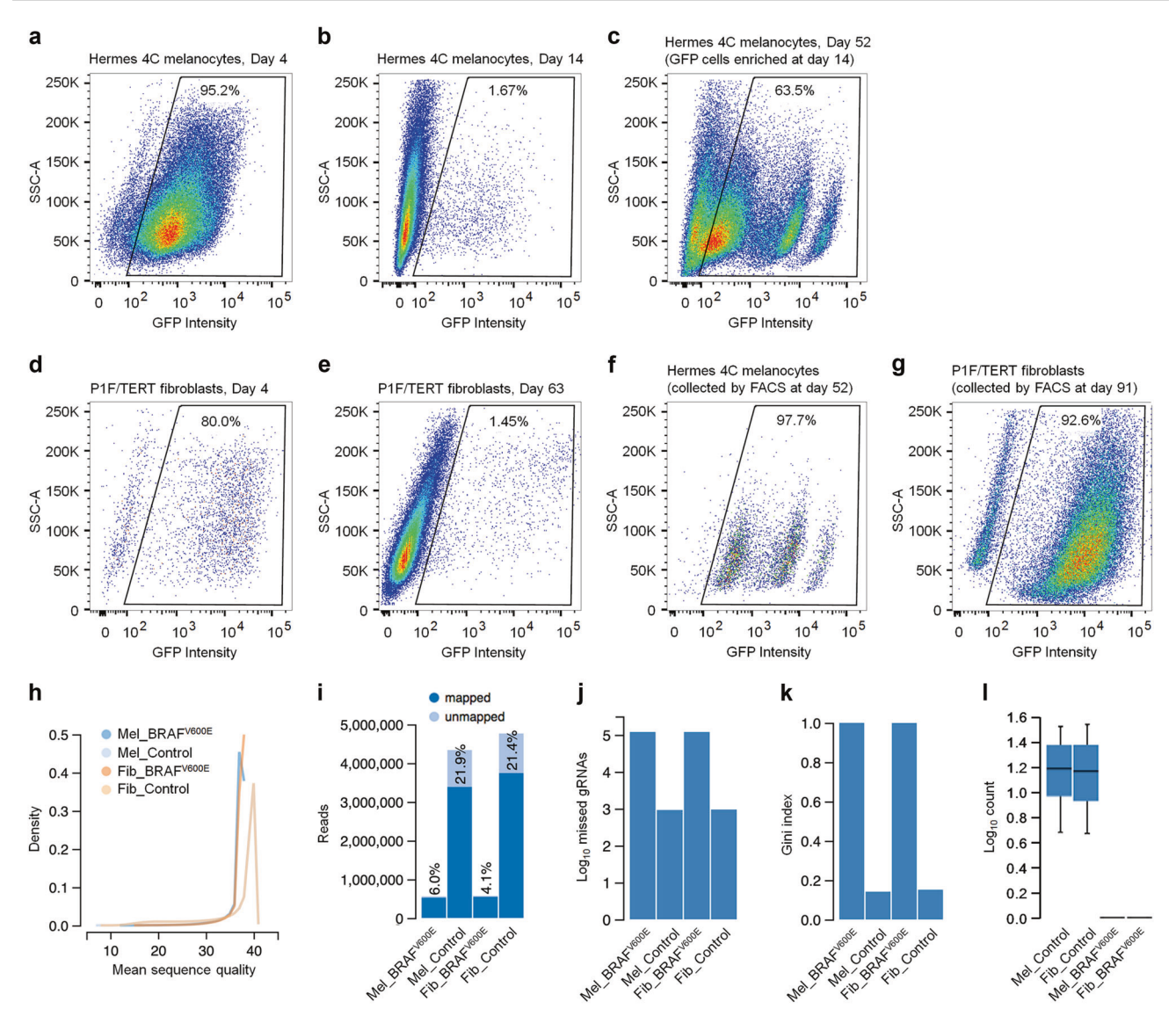


Fig. 2 GeCKO screening of genes whose disruptions enable cells to survive BRAF^{V600E} overexpression. **a–e** Flow cytometry analyses of GFP-positive human Hermes 4C melanocytes (**a–c**) and P1F/TERT fibroblasts (**d, e**) after EF–BRAF^{V600E}–GFP transduction. One week before the EF–BRAF^{V600E}–GFP transduction, the cells had been transduced with the GeCKO libraries (with transduction efficiencies of ~80%). **f, g** Flow cytometry analyses of FACS-collected GFP-positive Hermes 4C melanocytes (**f**) and P1F/TERT fibroblasts (**g**) 52 and 91 days, respectively, after EF–BRAF^{V600E}–GFP transduction. **h** Quality (Phred score) distribution of the sequencing reads of GeCKO sgRNA-

encoding sequences integrated in the genomes of melanocytes and fibroblasts. Mel_Control and Fib_Control are samples prepared from the melanocytes and fibroblasts, respectively, in the absence of EF-BRAF^{V600E}-GFP transduction. Mel_BRAF^{V600E} and Fib_-BRAF^{V600E} are samples prepared from the GFP-positive melanocytes and fibroblasts collected by FACS 52 and 91 days, respectively, after EF-BRAF^{V600E}-GFP transduction. i sgRNA reads perfectly mapped and unmapped to the GeCKO libraries. j Count of missing sgRNAs. k Gini-index of sgRNAs, which ranges between 0 and 1, and inversely correlates with sgRNA diversity. I Count distribution of sgRNAs

(Supplementary Table S2). Three of the 26 sgRNA-targeted genes, NPM1, VAV1, and ERK2 (also known as MAPK1) (Supplementary Table S2, shown in red), have been known to be implicated in cancer (COSMIC, https://cancer.sanger.ac.uk). Also, 15 of the 26 significantly enriched sgRNAs in the BRAF^{V600E}-overexpressing melanocytes were also significantly enriched in the BRAF^{V600E}-overexpressing P1F/TERT fibroblasts (Supplementary Tables S2 and S3, shown in bold).

Among the 187 sgRNAs (respectively targeting 187 different genes) detected in the BRAF^{V600E}-overexpressing P1F/TERT fibroblasts, 82 were significantly enriched (*p* value < 0.001 and FDR < 0.1) (Supplementary Table S3). Three of the 82 sgRNA-targeted genes, VAV1, ERK2, and CDKN1A (which encodes p21) (Supplementary Table S3, shown in red), have been known to be implicated in cancer (COSMIC, https://cancer.sanger.ac.uk). Of note, all the top ten enriched sgRNAs in the BRAF^{V600E}-overexpressing

fibroblasts were also significantly enriched in the BRAF^{V600E}-overexpressing Hermes 4C melanocytes (Supplementary Tables S2 and S3, shown in bold).

Only biallelic disruption of GPR4 or DBT enables the Hermes 4C melanocytes to be more tolerant to BRAF^{V600E} overexpression

sgRNAs targeting GPR4 and DBT were the most highly enriched in the Hermes 4C melanocytes overexpressing BRAF^{V600E} (Supplementary Table S2). GPR4 was also significantly enriched in the P1F/TERT fibroblasts (albeit to a lesser extent than in the melanocytes) overexpressing BRAF^{V600E} (Supplementary Table S3). GPR4 is a G protein-coupled receptor known to promote stress induced myocardial infarction [26] and renal parenchymal cell apoptosis [27], and inhibit tumor cell migration and metastasis [28]. DBT is a subunit of the branched-chain αketo acid dehydrogenase complex (BCKD), an innermitochondrial enzyme complex involved in the catabolism of branched-chain amino acids [29]. Mutation of DBT has been well-known to be implicated in maple syrup urine disease (MSUD) [30]. To date, however, the implications of GPR4 and DBT in oncogenic stress have not been documented.

To confirm the contribution of GPR4 or DBT disruption to increased tolerance of melanocytes to BRAFV600E overexpression, we transduced the Hermes 4C cells (~70% of the cells got transduced) with a lentiviral CRISPR/Cas9 vector encoding a GPR4- or DBT-targeting sgRNA under the U6 promoter, and the Cas9 and mCherry (a red fluorescent protein) under the EF1α promoter (Fig. 3a-c) [packaged from sgGPR4-mCherry and sgDBT-mCherry, respectively, (Supplementary Table S1)]. One week later, the cells were further transduced (also ~70% of the cells got transduced) with the EF-BRAF^{V600E}-GFP (Fig. 1a). Thirty days after the EF-BRAF^{V600E}-GFP transduction, GFPpositive cells accounted for ~7.1% and 6.4% of the GPR4and DBT-targeted cell populations, respectively (Fig. 3d, e). However, if the melanocytes had not been transduced with the GPR4- or DBT-targeting vector, no GFP-positive melanocytes could be detected two weeks after the EF-BRAF^{V600E}-GFP transduction. All the GFP-positive by 60 days collected FACS EF-BRAF V600E-GFP transduction were also mCherrypositive (Fig. 3f, g), indicating that all the cells that had survived the BRAF^{V600E} overexpression contained the GPR4- or DBT-targeting CRISPR/Cas9 vector. These results indicate that the CRISPR/Cas9-induced GPR4 or DBT disruption might have contributed to survival of the cells overexpressing BRAFV600E.

CRISPR/Cas9 disrupts a gene by inducing nucleotide insertions and/or deletions (indels) at its cutting site. A large

indel will likely disrupt an allele. However, if the indels are small, only biallelic frameshift indels, which occur with a probability of 4/9 (among all possible combinations of indels in two alleles of a cell), are likely to completely disrupt the gene. To examine if biallelic disruptions of GPR4 or DBT are required for the Hermes 4C melanocytes to become tolerant to BRAF^{V600E} overexpression, single GFP-positive cells were isolated 60 days after the EF-BRAF^{V600E}-GFP transduction, and the genomic DNA regions across the CRISPR/Cas9 cutting sites in the GPR4 and DBT genes were sequenced (from nucleotide -200 to nucleotide +200 relative to the CRISPR/Cas9 cutting sites, Fig. 3b, c). It turned out that 67 of the 68 (Supplementary Table S4) and 93 of the 94 (Supplementary Table S5) analyzed single GFP-positive cells targeted for GPR4 and DBT, respectively, contained biallelic disruptions of the targeted genes. In contrast, 4 of the 9 (Supplementary Table S6) and 5 of the 15 (Supplementary Table S7) analyzed single control (without BRAF^{V600E} expression) cells targeted for GPR4 and DBT, respectively, contained biallelic disruptions of the targeted genes. These results indicate that in the absence of BRAF^{V600E} expression biallelic disruption of GPR4 or DBT conferred no advantage of cell growth. However, biallelic disruption of DBT or GPR4 enabled the melanocytes to be more tolerant to BRAF^{V600E} overexpression.

Mutations of GPR4 or DBT are rare in cancers

By using the cBioPortal [31], we analyzed GPR4 and DBT mutations in cancers based on data collected in TCGA (The Cancer Genome Atlas) [32]. Mutations of these genes are rare (Supplementary Fig. S1) and not considered driver mutations in all current cancer databases, such as COSMIC.

Significant downregulation of GPR or DBT is uncommon in cancers

We used GEPIA (Gene Expression Profiling Interactive Analysis) [33] to analyze expressions of GPR4 and DBT in 23 cancer types which have matched RNA-Seq data of normal tissues available in TCGA. The level of GPR4 expression is significantly (p < 0.01) lower in 5 and higher in 2 of the 23 cancer types than in the matched normal tissues (Supplementary Fig. S2A). The level of DBT expression is significantly lower in 4 of the 23 cancer types than in the matched normal tissues (Supplementary Fig. S2B). Note that for certain cancer types, such as skin cutaneous melanoma (SKCM), the available RNA-Seq data for matched normal tissues are too limited to make a meaningful comparison. Still, it appears that significant downregulation of GPR4 or DBT is

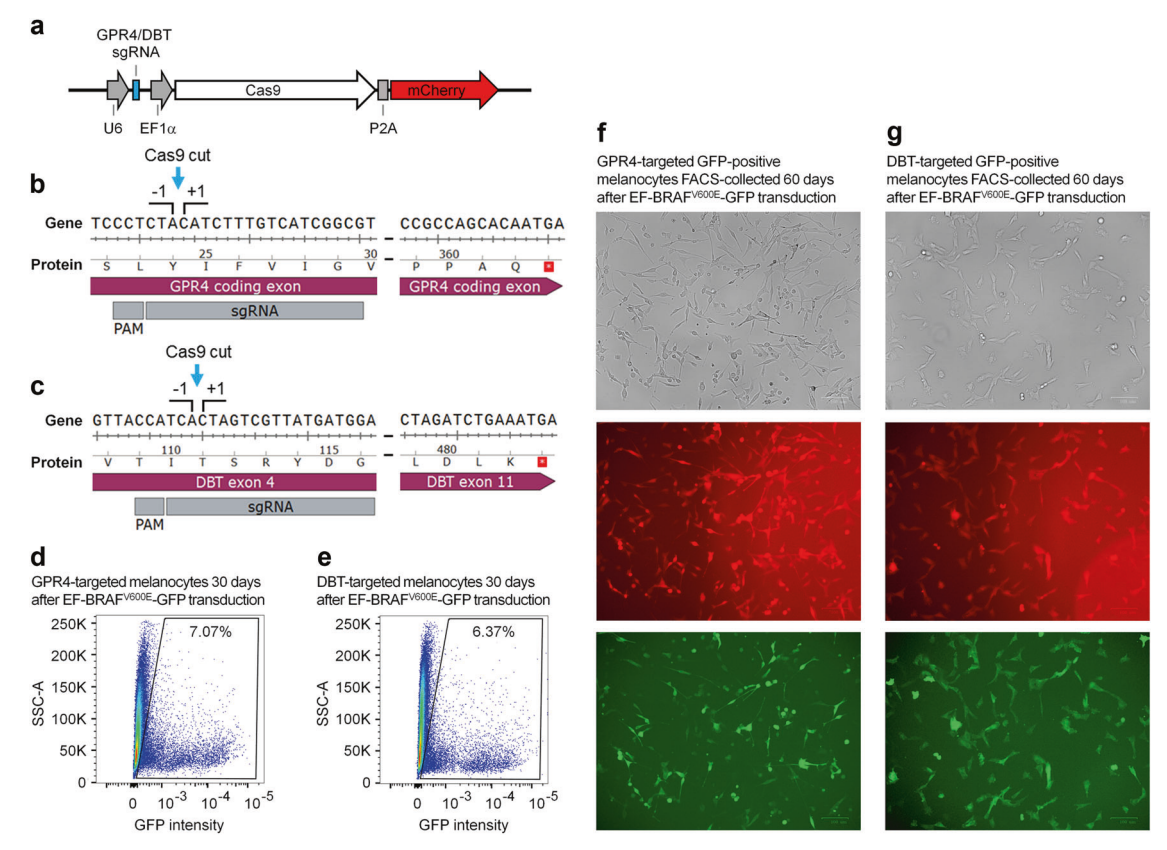


Fig. 3 Transduction of GPR4- or DBT-targeting CRISPR/Cas9 enables survival of a fraction of Hermes 4C melanocytes over-expressing BRAF^{V600E}. **a** Structure of the lentiviral vector with GPR4- or DBT-targeting CRISPR/Cas9 cassette. **b**, **c** CRISPR/Cas9 targeting sites in the GPR4 gene (which has a single protein-coding exon) (**b**) and the DBT gene (which has 11 protein-coding exons) (**c**). **d**, **e** Flow cytometry analyses of GPR4- (**d**) and DBT-targeted (**e**) melanocytes

30 days after EF–BRAF^{V600E}–GFP transduction. One week before EF–BRAF^{V600E}–GFP transduction, the cells had been transduced with the GPR4- or DBT-targeting CRISPR/Cas9. **f**, **g** Bright-field (top), red (middle), and green fluorescence images of GFP-positive GPR4-(**f**) and DBT-targeted (**g**) melanocytes collected by FACS 60 days after EF–BRAF^{V600E}–GFP transduction

uncommon in cancers although it may occur in several cancer types.

The expression level of BRAF positively correlates with that of GPR4 in most cancer types, and with that of DBT in all cancer types

We wondered if the expression of GPR4 or DBT is correlated with that of BRAF. We performed the analyses by using Xena [34] and the UCSC Toil RNAseq Recompute Data Hub (https://xena.ucsc.edu/). The expression level of BRAF is somewhat negatively correlated with that of DBT (Spearman's rank rho = -0.2789) but not with that of GPR4 (Spearman's rank rho < 0.1) in normal tissues as a whole (Fig. 4a, d, e). However, weak to moderate negative or positive correlations of BRAF expression with DBT and GPR4 expressions can be seen in several types of normal tissues (Supplementary Table S8). Intriguingly, from weak to strong positive correlations between BRAF and DBT expressions can be seen in all cancer types including SKCM

(Fig. 4b, c, f, and h; Supplementary Table S9). Weak to moderate positive correlations between BRAF and GPR4 expressions can also be seen in most (26 of 33) cancer types (Fig. 4b, g; Supplementary Table S9), but not in SKCM and six other cancer types (Fig. 4c, i; Supplementary Table S9).

BRAF^{V600E} is commonly found in SKCM and thyroid carcinomas [11]. BRAF^{V600M} is also substantially found in SKCM. In the melanomas, expressions of all the different forms of BRAF, wild type and the BRAF^{V600E} and BRAF^{V600M} mutants, appear to be positively correlated with that of DBT but not necessarily with that of GPR4 (Supplementary Fig. S3). In thyroid carcinomas, expressions of both the wild-type BRAF and BRAF^{V600E} are positively correlated with those of DBT and GPR4 to different extents (Supplementary Fig. S4).

Taken together, our observations suggest that the level of BRAF, either wild type or the BRAF V600E and BRAF V600M mutants, needs to be balanced with that of GPR4 in most cancer types, and with that of DBT in all cancer types.

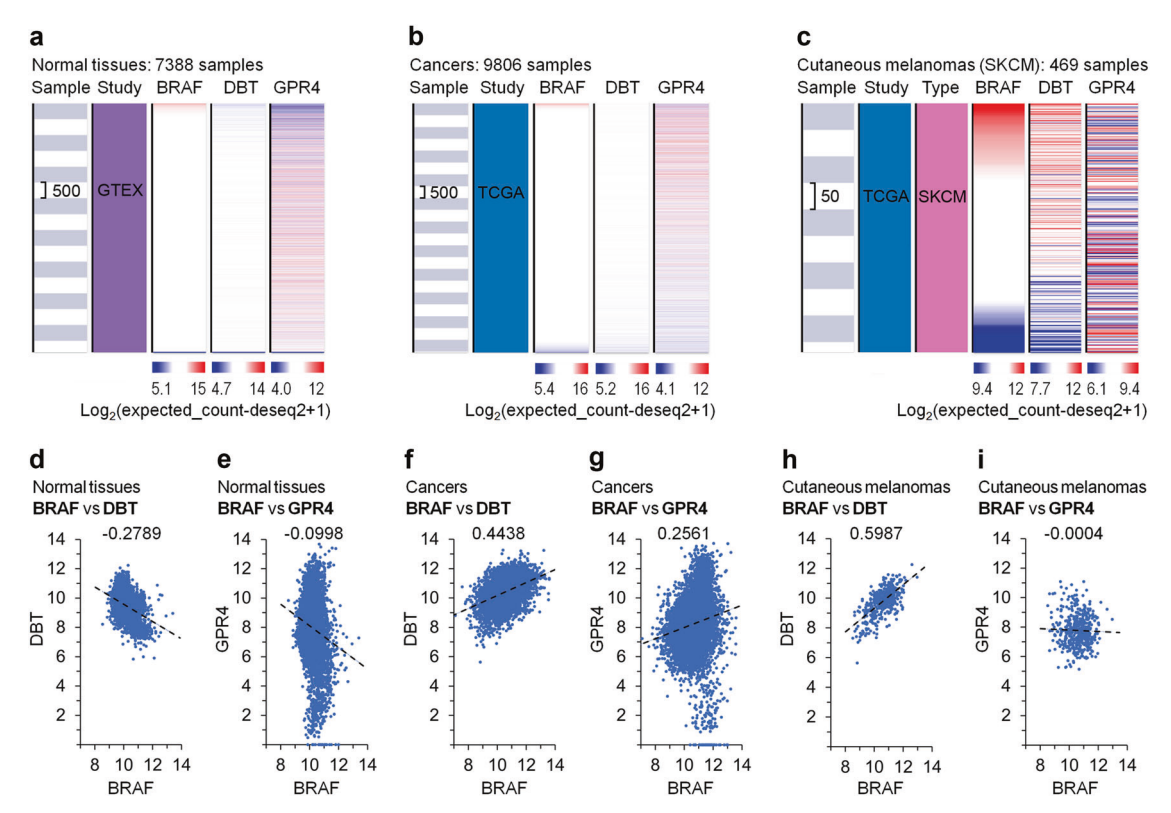


Fig. 4 Correlations of BRAF expression with DBT and GPR4 expressions. **a–c** Visual spreadsheet showing expression levels of BRAF, DBT, and GPR4 (sorted from high to low for the expression levels of BRAF) in normal tissue (**a**), cancer (Pan-Cancer) (**b**), and skin cutaneous melanoma (SKCM) (**c**) samples. **d–i** Scatter plots showing correlations of BRAF expression with DBT and GPR4 expressions in the indicated samples. Expression levels are shown as RSEM expected counts normalized with DESeq2 [log₂(expected_count-deseq2 + 1)]. Numbers above plots are Spearman's rank rho

values, which in the rages of 0.1–0.39, 0.4–0.69, and 0.7–1.0 are considered to be weak, moderate, and strong positive correlations, respectively, and those of -0.1 to -0.39, -0.4 to -0.69, and -0.7 to -1.0 to be weak, moderate, and strong negative correlations, respectively. The RNA-Seq data of normal tissues and cancers in GTEX (Genotype-Tissue Expression) and TCGA (The Cancer Genome Atlas), respectively, were analyzed through the UCSC TOIL RNAseq Recompute Data Hub on UCSC Xena (https://xena.ucsc.edu/)

Disruption of DBT in the Hermes 4C melanocytes attenuates p14^{ARF}, p15^{INK4b}, p16^{INK4a}, p53 activation, and apoptosis

In view of the findings that expression of BRAF is positively correlated with that of DBT in all cancer types including melanoma, we decided to focus on elucidating how DBT functions. Single Hermes 4C melanocytes with biallelic frameshift indels of DBT (DBT^{-/-}) were isolated (following transduction of the cells with the DBT-targeting lentiviral CRISPR/Cas9 vector as shown in Fig. 3a, c) and grown into clones in conditional media. To make sure that the observed results are indeed due to disruption of DBT, rather than an unintended off-target gene, we complemented the DBT^{-/-} cells with a lentiviral vector expressing the DBT cDNA [packaged from EF-DBT-BSD (Supplementary Table S1)]. To prevent the cDNA from being targeted by the DBT-targeting CRISPR/Cas9, silent mutations were introduced into the cDNA (Fig. 5a). The level of DBT protein in the cDNA-complemented DBT^{-/-} cells is ~2 times higher than that in the wild-type cells (Fig. 5b). Upon EF–BRAF^{V600E}–GFP transduction, the wild type and cDNA-complemented DBT^{-/-} cells showed significantly high levels of apoptosis compared to the uncomplemented DBT^{-/-} cells (Fig. 5c), indicating that the enhanced tolerance to BRAF^{V600E} overexpression is indeed due to disruption of DBT rather than an off-target.

Oncogenic stresses can activate signaling pathways that lead to cellular apoptosis or senescence (Fig. 5d) [3, 8, 23]. We examined whether disruption of DBT affected the levels of key proteins in the signaling pathways. Total p53, more significantly serine-15 phosphorylated p53 (p-p53) which results from the kinase activity of ERK1/2 [35, 36], were upregulated in wild type but not DBT^{-/-} cells upon BRAF^{V600E} overexpression (Fig. 5e). Complementation of the DBT^{-/-} cells with the DBT cDNA restored p53 and p-p53 upregulation upon BRAF^{V600E} overexpression (Fig. 5e).

p14^{ARF}, a tumor suppressor protein, positively regulates p53 by interacting with and inhibiting the ubiquitin ligase

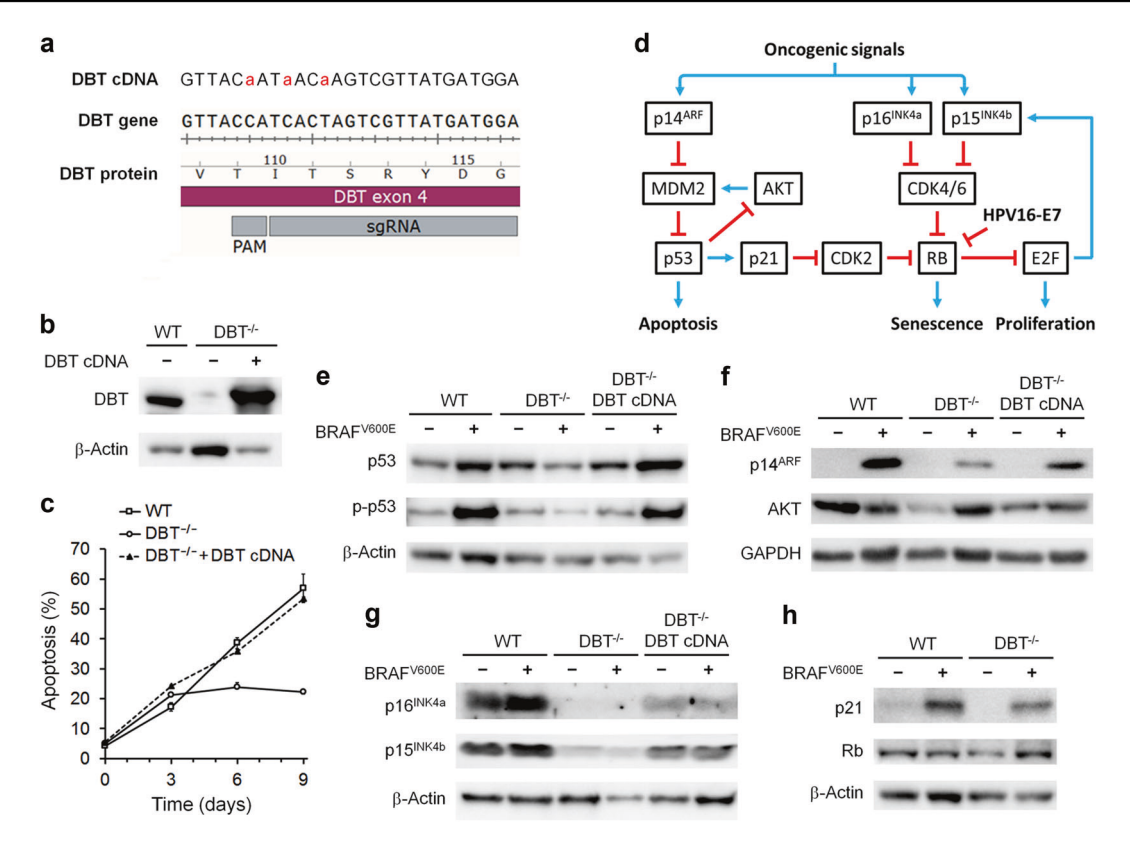


Fig. 5 Disruption of DBT in the Hermes 4C melanocytes disturbes the signaling arm that leads to p53 activation and cellular apoptosis, but does not significantly affect the p21 and Rb signaling arm that leads to cellular senescence. **a** Silent mutations introduced into the DBT cDNA (shown in red small case letters) of the lentiviral transfer vector EF-DBT-BSD (Supplementary Table S1). **b** Western blot

showing levels of DBT protein. **c** Cell apoptosis following EF–BRAF V600E –Hyg transduction. **d** Simplistic schematic of signaling pathways leading to cellular apoptosis and senescence in response to oncogenic stress. **e–h** Western blots showing levels of key proteins implicated in the signaling pathways. β -actin and GAPDH serve as loading controls

MDM2 (Fig. 5d) [37]. In agreement with previous reports showing that p14ARF is induced by increased mitogenic stimuli conveyed by oncogenes [38, 39], p14ARF was highly induced in wild-type cells upon BRAFV600E overexpression (Fig. 5f). The induction was greatly compromised in the DBT^{-/-} cells and complementation of the cells with the DBT cDNA partially restored the induction (Fig. 5f). In contrast to p14 ARF, AKT negatively regulates p53 by phosphorylating and activating MDM2 [40]. AKT level was high in the wildtype cells but low in the DBT^{-/-} cells (Fig. 5f). Upon BRAF^{V600E} overexpression, AKT was downregulated in the wild type but upregulated in the DBT^{-/-} cells (Fig. 5f). Of note, the levels of AKT in the wild type and DBT^{-/-} melanocytes appear to inversely correlate with those of the phosphorylated p53, which is likely due to the negative feedback regulation of AKT by p53 (Fig. 5d) [41]. Complementation of the DBT^{-/-} cells with the DBT cDNA partially restored the AKT levels (Fig. 5f).

The tumor suppressor proteins p15^{INK4b} and p16^{INK4a} were high and slightly upregulated in the wild-type Hermes 4C melanocytes upon BRAF^{V600E} overexpression (Fig. 5g), presumably due to the constitutive suppression of Rb by

HPV16-E7, which derepresses E2F for stimulating expressions of p15^{INK4b} and p16^{INK4a} in these cells (Fig. 5d). However, these proteins were essentially undetectable in the DBT $^{-/-}$ cells with or without BRAF V600E overexpression (Fig. 5g). Also, complementation of the DBT $^{-/-}$ cells with the DBT cDNA partially restored the levels of p15^{INK4b} and p16^{INK4a} (Fig. 5g).

In normal cells, p21, a potent universal inhibitor of cyclin dependent kinases (CDKs), is tightly controlled by p53 in response to genotoxic stimuli [42]. However, p21 can also be strongly induced in a p53-independent manner [43]. As expected, p21 was induced in the wild-type melanocytes upon BRAF^{V600E} overexpression (Fig. 5h). Interestingly, p21 was also induced by BRAF^{V600E} overexpression in the DBT^{-/-} cells (Fig. 5h), which showed defective upregulation of p53 in response to BRAF^{V600E} overexpression (Fig. 5e). This indicates that p21 upregulation in the DBT^{-/-} cells is largely independent of p53. Also, the levels of Rb were similar in the wild-type and DBT^{-/-} cells and were not significantly affected by BRAF^{V600E} overexpression (Fig. 5h).

Taken together, our results indicate that disruption of DBT in the Hermes 4C melanocytes disturbes the signaling arm

that leads to p53 activation and cellular apoptosis. On the other hand, the p21 and Rb signaling arm that leads to cellular senescence appears to be less affected, although the disruption attenuated the expressions of p15^{INK4b} and p16^{INK4a}. As mentioned above, this can be due to the constitutive suppression of Rb by HPV16-E7 in the melanocytes.

Disruption DBT in the Hermes 4C melanocytes severely attenuates ERK/MAPK signaling at least in part due to accumulation of branched chain α -keto acids

BRAF-implicated ERK/MAPK signaling involves activation and negative feedback regulations (Fig. 6a) [44, 45]. The absence of increased serine-15 phosphorylation of p53, which is catalyzed by ERK1/2 [35, 36], in DBT^{-/-} melanocytes upon BRAF^{V600E} overexpression (Fig. 5e), plus our observation that the expression level of BRAF is positively correlated with that of DBT in all cancer types suggest that DBT may play a role in the ERK/MAPK signaling. Indeed, the level of native BRAF protein in the DBT^{-/-} cells was ~1/3 that in the wild-type cells (Fig. 6b, c, compare the BRAF bands in the 'U' lanes between the two cell types). Interestingly, the ectopically expressed BRAFV600E in the DBT^{-/-} cells was also less than half of that in the wild-type cells (Fig. 6b, c). However, the levels of total and phosphorylated MEK in the DBT^{-/-} cells were similar to those in the wild-type cells (Fig. 6b, c), presumably due to severely attenuated negative feedback regulation of MEK phosphorylation in the mutant cells (see below). The level of phosphorylated ERK2 in the DBT^{-/-} cells was consistently ~1/2 that in the wild-type cells (repeated 3 times) (Fig. 6b, c).

The tyrosine and serine/threonine dual-specificity MAPK phosphatases (DUSPs) are the targets of transcriptional induction and negative feedback regulators of ERK/MAPK signaling (Fig. 6a) [44, 45]. Among the multiple phosphatases, DUSP4, DUSP5, and DUSP6 are solely transcriptionally induced by phosphorylated ERK1/2 [44]. DUSP4 level was high and upregulated upon ectopic overexpression of BRAF^{V600E} in the wild-type cells but virtually undetectable in the DBT^{-/-} cells (Fig. 6d). This indicates that the ERK/MAPK signaling is severely attenuated even when BRAFV600E is ectopically overexpressed in the DBT^{-/-} cells. On the other hand, the levels of DUSP5 and DUSP6 were slightly higher in the DBT^{-/-} cells than in the wild-type cells upon the ectopic $BRAF^{V600E}$ expression (Fig. 6d). The reason for the slight upregulation of DUSP5 and DUSP6 in the DBT-/- cells was not explored further, but could be a compensation for the dramatically reduced DUSP4. The extremely low level of DUSP4 in the DBT^{-/-} cells would exert a very low level of negative feedback regulations of the signaling pathway, which may explain why the levels of phosphorylated MEK and ERK were essentially unchanged and moderately attenuated, respectively, in the DBT $^{-/-}$ cells (Fig. 6b, c). The severely attenuated ERK/MAPK signaling also nicely explains why the levels of p14 $^{\rm ARF}$, p16 $^{\rm INK4a}$, p15 $^{\rm INK4b}$, and phosphorylated p53 were so low in DBT $^{-/-}$ cells even after BRAF $^{\rm V600E}$ overexpression (Fig. 5e–g).

The first step of the catabolism of branched amino acids is catalyzed by branched-chain amino acid aminotransferase, producing the branched chain α -keto acids, α -ketoisocaproic acid (KIC), α-ketomethylvaleric acid (KMV), and α-ketoisovalerate (KIV) from leucine, isoleucine, and valine, respectively (Fig. 6e) [46, 47]. Along with other subunits of BCKD, DBT is required for the second and ratelimiting step of the catabolism. Disruption of DBT will cause accumulation of KIC, KMV, and KIV. KIC and its precursor leucine, which accumulate most in MSUD (reaching a plasma concentration of 5 mM), are considered the main toxins associated with the disease [48]. The levels of ERK2 phosphorylation was inversely related to the levels of KIC (Fig. 6f), indicating that the attenuation of ERK2 phosphorylation upon DBT disruption is at least in part due to accumulation of the branched chain α -keto acids.

In normal cells, 95% of KIC is catabolized into isovaleryl-CoA by BCKD and the rest 5% of the metabolite is converted to hydroxy methyl butyrate (HMB) by KIC dioxygenase (KICDO) [49] (Fig. 6e). In theory, disruption of DBT may also cause a certain level of HMB accumulation in the cell. However, treatment of the cells with HMB did not significantly affect ERK2 phosphorylation (Fig. 6g), indicating that HMB does not substantially affect ERK/MAPK signaling.

Overexpression of DBT kills melanoma cells regardless of the presence of $\mathsf{BRAF}^{\mathsf{V600E}}$ mutation

We tested if overexpression of DBT could kill melanoma cells. Melanoma cell lines SK-MEL-23 and MM485, which have wild-type BRAF, and 451-Lu and COLO-800, which have the BRAF^{V600E} mutation, were transduced with a lentiviral vector expressing mCherry (EF-mCherry, as a control) or DBT and mCherry (EF-DBT-mCherry) under the EF1 α promoter (Fig. 7a). As expected, transduction with EF-mCherry caused little (<5%) cell death even after prolonged culturing (Fig. 7b, and data not shown). Intriguingly, transduction with EF-DBT-mCherry killed ~95% of the SK-MEL-23 cells within 4 days (Fig. 7c). Fourteen days after the EF-DBT-mCherry transduction, a large fraction of the mCherry-positive MM485, 451-Lu, and COLO-800 melanoma cells were killed and the survived ones looked "unhealthy" (enlarged and/or dying) (Supplementary Fig. S5), indicating that they can also be killed by DBT overexpression albeit at a slower pace compared with SK-MEL-23 cells. In contrast to melanoma cells, the Hermes 4C

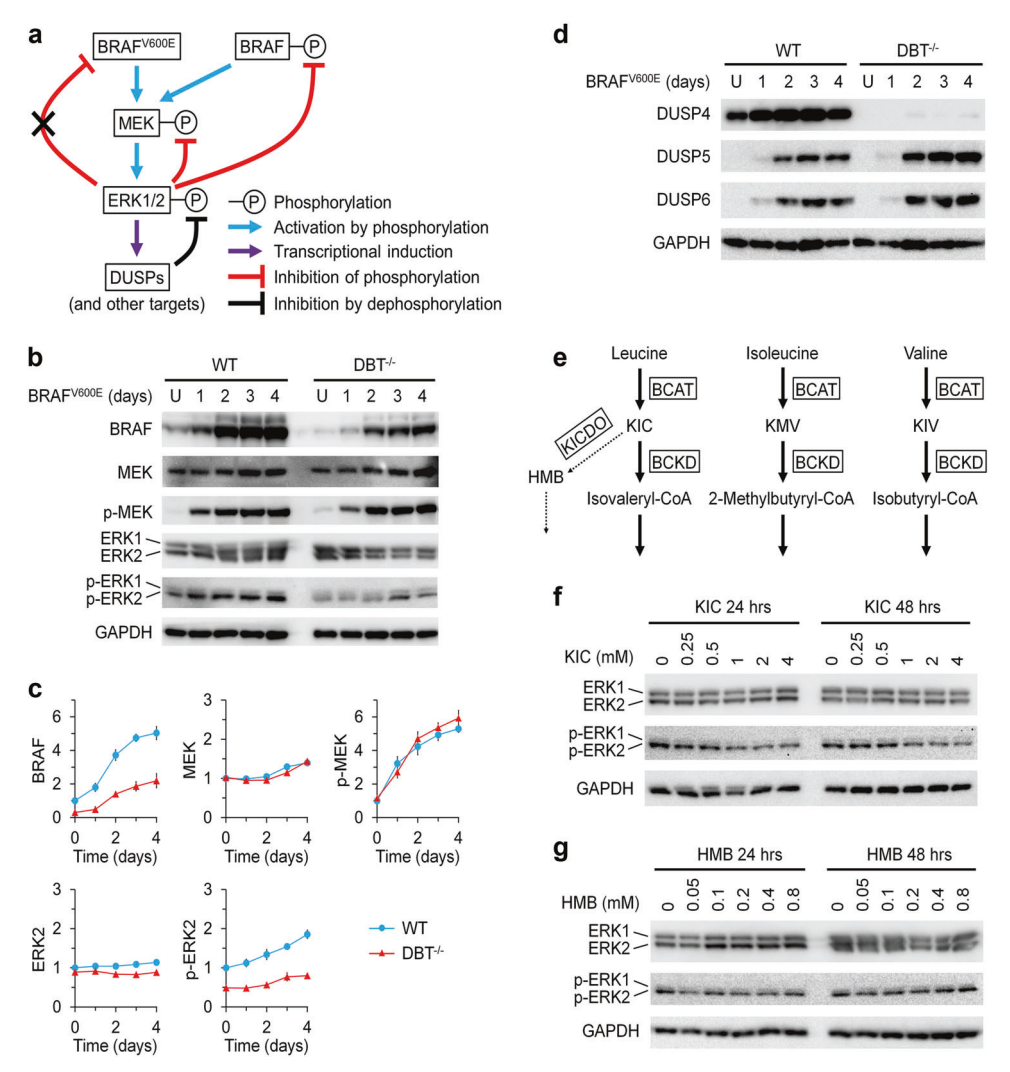


Fig. 6 Disruption of DBT severely attenuates ERK/MAPK signaling at least in part due to accumulation of branched chain α-keto acids. **a** Simplistic schematic showing regulation of BRAF-implicated ERK/MAPK signaling. **b** Western blots showing levels of total BRAF, and total and phosphorylated MEK and ERK1/2 in the wild type (WT) and DBT $^{-/-}$ Hermes 4C melanocytes before (U) and at different days after EF–BRAF V600E –GFP transduction. **c** Plots showing levels of the indicated proteins in the WT and DBT $^{-/-}$ melanocytes at different days after EF–BRAF V600E –GFP transduction. The level of each of the proteins in the untransduced (U) WT cells is presented as 1, and those in the other samples are

normalized to that in the untransduced WT cells. Error bars stand for standard errors. **d** Western blots showing levels of DUSP4, DUSP5, and DUSP6 in the WT and DBT^{-/-} melanocytes. **e** Schematic showing the first two steps of the catabolism of branched chain amino acids. **f** Western blots showing the levels of total and phosphorylated ERK1/2 in Hermes 4C melanocytes following treatments with KIC at the indicated concentrations and durations. **g** Western blots showing the levels of total and phosphorylated ERK1/2 in Hermes 4C melanocytes following treatments with HMB at the indicated concentrations and durations

melanocytes showed slow growth but were not significantly killed following transduction with EF-DBT-mCherry (not shown).

Discussion

Through unbiased genome-wide screening, we identified genes whose disruptions enhance tolerance of human cells to $BRAF^{V600E}$ expression. Besides confirmation of the top

selected genes, our screening results are supported by the observations that a large fraction of the genes are shared by the melanocytes and fibroblasts. Of note, the genes include the proto-oncogenes ERK2, a key kinase downstream of MEK [50], and VAV1, a guanine nucleotide exchange factor for Rho family GTPases that also activates the ERK/MAPK signaling pathway [51–54]. Our results are in line with previous findings that attenuation of ERK/MAPK signaling, by genetic inactivation of ERK2, RNAi-mediated knockdown of ERK1 or ERK2, or MEK inhibitors, prevents

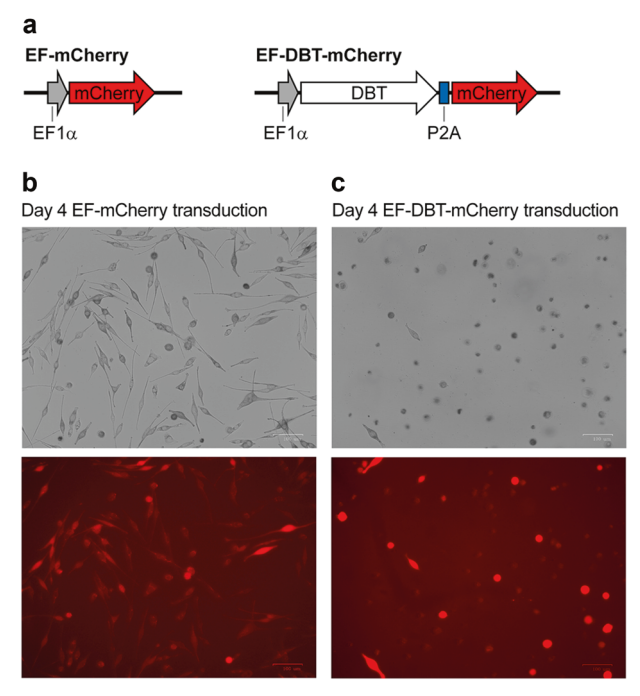


Fig. 7 Overexpression of DBT quickly kills SK-MEL-23 melanoma cells. (a) Structures of lentiviral vectors EF-mCherry and EF-DBT-mCherry. (b and c) Bright field (top) and red fluorescence (bottom) images of SK-MEL-23 melanoma cells 4 days after transduction with EF-mCherry (b) and EF-DBT-mCherry (c)

the activation of senescence, allowing oncogenic RAS to transform primary cells [55].

IL-6 and CXCR2 have been reported to be required for BRAF^{V600E} induced senescence or apoptosis [16, 17]. However, disruptions of the two genes were not significantly selected in either the melanocytes or the fibroblasts we used upon $BRAF^{V600E}$ overexpression. This is not due to the lack of IL-6- and CXCR2-targeting sgRNAs in the GeCKO libraries we used, as plenty of these sgRNAs were present in the control cells (which were transduced with the GeCKO libraries but not the EF-BRAF^{V600E}-GFP). Our screening relies on disruption of genes, which may miss the identification of genes whose targeting sgRNAs have low genedisruption efficiency or whose disruptions cause cell lethality or poor growth. In contrast, the previous reports used siRNA knockdown, which allows the identification of genes whose reduced expressions enable more tolerance to BRAF V600E expression. It should also be noted that our screening will miss the genes whose activation (rather than disruption) will enable the cell to escape from oncogeneinduced senescence or apoptosis, such as activation of genes in the PI3K signaling pathway [18].

We showed that disruption of GPR4 was the most highly selected in the melanocytes and moderately selected in the fibroblasts we used upon BRAF^{V600E} overexpression (Supplementary Tables S2 and S3). GPR4 appears to have multifaceted roles in cell proliferation, apoptosis, and

oncogenesis, presumably depending on cell types and local environments. GPR4 has been shown to be an oncogenic factor [56, 57]. GPR4 also appears to be a proapoptosis factor, as it promotes myocardial infarction [26], mediates endoplasmic reticulum stress leading to inflammation and apoptosis [58], and causes enhanced renal parenchymal cell apoptosis [27]. Also, GPR4 has been shown to constitutively suppress ERK1/2 activation [59]. It is unlikely that disruption of GPR4 enhances BRAF^{V600E} tolerance by derepressing ERK1/2, as the disruption should in theory exacerbate the cellular stress caused by BRAF^{V600E} over-expression (which activates ERK1/2). Rather, disruption of GPR4 may enhance BRAF^{V600E} tolerance by attenuating cellular apoptosis through a mechanism that remains to be elucidated.

Our screening results indicate that certain genes are specifically selected in the melanocytes or fibroblasts we used upon BRAF^{V600E} overexpression. Of note, CDKN1A, which encodes the cyclin-dependent kinase inhibitor p21, has been well-known to be the major regulator of fibroblast senescence, as loss of p21 in fibroblasts causes bypass of senescence [60]. Unlike fibroblasts, melanocytes appear to utilize a CDKN1A-independent mechanism for cellular senescence [61]. In line with these previous findings, we found that disruption of CDKN1A is highly selected upon BRAF^{V600E} overexpression in the fibroblasts but not in the melanocytes (Supplementary Tables S2 and S3).

To date, little has been known about the roles of DBT in biochemical or cellular processes except for its requirement for catalyzing the second and rate-limiting step of branched amino acid breakdowns. Here, we discovered that disruption of DBT severely attenuates ERK/MAPK signaling at least in part due to accumulation of branched chain α-keto acids. Signal propagation through the ERK/ MAPK cascade is facilitated by scaffold proteins such as KSR, Paxillin, and IQGAP1 [62]. Particularly, IQGAP1 has been known to bind to and be implicated in the activation of both MEK1/2 and ERK1/2 [63]. The severely attenuated ERK/MAPK signaling in DBT^{-/-} cells may not be solely due to the ~threefold downregulation of BRAF, but may also be partially achieved by directly inhibiting the activities of the ERK/MAPK signaling kinases and/or by interfering the interactions of the kinases with the scaffold proteins. Future studies will be needed to clarify the underlying mechanisms.

Our findings that DBT is implicated in ERK/MAPK signaling and sensitivity of melanocytes to BRAF^{V600E} overexpression may open up new avenues of research regarding the initiation and development of melanomas, as well as other cancers related to BRAF^{V600E} expression and activation of ERK/MAPK signaling. Also, treatments of melanoma with BRAF and MEK inhibitors have shown unprecedented survival responses [64]. However, the

responses are generally transient, with a median time to progression of 5.1–8.8 months. The acquired resistance has been found to be due to reactivation of the ERK/MAPK pathway and to a lesser extent the PI3K–Akt pathway [64]. Our findings that expression of BRAF positively correlates with that of DBT in all cancer types and overexpression of DBT kills all four melanoma cell lines tested may open up novel strategies for treating melanomas and other types of cancers.

Finally, a large fraction of the genes that were significantly selected upon BRAF^{V600E} overexpression in the melanocytes and fibroblasts we used (Supplementary Tables S2 and S3) have not been previously recognized as being implicated in oncogenic stresses. Future characterizations of these genes may also shed more lights on the underlying mechanisms of tumorigenesis and open up more treatment options.

Materials and methods

Cell lines

Human Hermes 4C melanocytes, which were immortalized by expressing human telomerase (TERT) and HPV16-E7 protein, and melanoma cell lines 451-Lu, COLO-792, COLO-800, MM485, SK-MEL-23, and WM-1158 were kindly provided by the Wellcome Trust Functional Genomics Cell Bank. The melanocytes were cultured in RPMI1640-GlutaMax medium supplemented with 10% newborn calf serum, 10 ng/ml human stem cell factor, 200 nM phorbol 12-myristate 13-acetate, 200 pM cholera toxin, and 10 nM endothelin 1. The melanoma cell lines were cultured in RPMI1640-GlutaMax medium supplemented with 10% of fetal calf serum. Human P1F/TERT fibroblasts, which were immortalized by expressing human TERT, were obtained from the Rheinwalk Lab of Harvard Skin Disease Research Center and cultured in DMEM/F12 medium supplemented with 15% newborn calf serum and 10 ng/ml of epidermal growth factor.

Lentiviral vectors

All lentiviral transfer vectors used in this study were created by using the backbone of lentiCRISPR v2, an improved lentiviral transfer vector that has high functional viral titer and was used for creating the GeCKO, v2 libraries [24] (Supplementary Table S1). The DNA of GeCKO, v2 libraries were purchased from Addgene (1000000048) and transformed into Endura electrocompetent *Escherichia coli* cells (Lucigen, 60242) to obtain $\sim 2 \times 10^8$ independent colonies.

To package the lentiviral vectors, the purified DNA of a lentiviral transfer vector was cotransfected with that of the envelope vector pCMV-VSV-G (Addgene, 8454) and packaging vector psPAX2 (Addgene, 12260) into HEK293T cells (Clontech, 632180) by using the calcium phosphate coprecipitation method [65]. A total of 1.5 μ g plasmid DNA with the ratio of transfer vector, pCMV-VSV-G and psPAX24 being 4:1:3 was used for transfecting a well of 12-well plates. Lentiviral particles were harvested 48 h after the transfection and concentrated by ultracentrifugation at 24 000 RPM for 2 h at 4 °C.

Genome-wide screening of genes implicated in cellular sensitivity to BRAF^{V600E} expression

Ten million Hermes 4C or P1F/TERT cells were suspended in 24 ml of medium containing packaged lentiviral particles of the GeCKO, v2 libraries and 8 µg/ml of polybrene. The cells were aliquoted into the wells of two 12-well plates and spun at 2000 RPM for 2 h at room temperature. After overnight incubation in 37 °C incubators filled with 10% (for melanocytes) or 5% (for fibroblasts) CO₂, the cells were reseeded in T-75 flasks. About 80% of the cells were transduced by the GeCKO libraries. One week after the GeCKO library transduction, the cells were pooled and half of them were stored as control and the other half were further transduced with lentiviral particles packaged with EF-BRAF^{V600E}-GFP (Supplementary Table S1). During the period of further culturing, the GFP-positive cells were analyzed by flow cytometry and enriched by using FACS. At the end of the screening (52 and 91 days after the EF-BRAF^{V600E}-GFP transduction of Hermes 4C and P1F/ TERT, respectively), the GFP-positive cells were collected by FACS. Genomic DNA was isolated from the control and collected GFP-positive cells by using the Blood & Cell culture DNA midi Kit (Qiagen, #13343).

To analyze the profiles of sgRNAs in the control and collected GFP-positive cells, three rounds of PCR across the integrated sgRNA-encoding sequences were performed by using Herculase II Fusion DNA Polymerase (Agilent, #600675). The 1st round PCR had 24 cycles and used primers Lenti-F1 and Lenti-R1 (Supplementary Table S10), and 1 or 120 µg (in 12 tubes of reaction) of genomic DNA from the GFP-positive or control cells, respectively. The PCR products of 400-600 bp in the same group were combined and gel purified. The 2nd round PCR had 21 cycles and used primers GECKO-1 and GECKO-2 (Supplementary Table S10), and the gelpurified DNA from the 1st round PCR. The 3rd round PCR, which was aimed at adding index (barcodes) and additional sequences required for Illumina sequencing, had six cycles and used Tru-U as the forward primer and Tru-B1, B2, B3, or B4 (Supplementary Table S10) as the reverse primer for the different cell groups. The sequencing was carried out on a Hi-Seq 2000 sequencing platform and the data was analyzed by using MAGeCK-VISPR [66].

Analysis of CRISPR/Cas9-induced DBT and GPR4 indels in single Hermes 4C melanocytes with or without BRAFV600E overexpression

One hundred thousand Hermes 4C melanocytes were transduced with lentiviral particles packed with sgDBTmCherry or sgGPR4-mCherry (Supplementary Table S1). The amount of the lentiviral particles was titrated so that ~70% of the cells got transduced. One week after the transduction, the cells were pooled and half of them were served as control and the other half were further transduced with the lentiviral particles packaged EF-BRAF^{V600E}-GFP (Fig. 1a) (also ~70% of the cells got transduced). Thirty days after EF-BRAF V600E-GFP transduction, GFP-positive cells were enriched by FACS. After further culturing for another month (i.e., 60 days after EF-BRAF^{V600E}-GFP transduction), single GFP-positive cells were deposited into individual wells of 96-well plates by FACS. The 400 bp region across the CRISPR/ Cas9 cutting site (200 bp upstream and downstream) of the DBT and GPR4 gene in each of the individual cells were sequenced. To create the sequencing templates, three rounds of PCR were performed. The 1st round PCR had 31 cycles and used primers DBT-F2 and DBT-R2 for the DBT gene or GPR4-F2 and GPR4-R2 for the GPR4 gene (Supplementary Table S11). The 2nd round PCR had 35 cycles and used primers DBT-Tru-U and DBT-Tru-Seq for the DBT gene and GPR4-Tru-U and GPR4-Tru-Seq for the GPR4 gene (Supplementary Table S11). The 3rd round PCR had 20 cycles and used primer Tru-U1-8 respectively paired with Tru-B1-12 (96 different combinations) (Supplementary Table S11) for the different individual cells. The final round PCR products were sequenced on an Illumina Miseq platform. The DBT and GPR4 gene regions across the CRISPR/Cas9 cutting site in the control cells (transduced with sgDBT-mCherry or sgGPR4-mCherry but not EF-BRAF^{V600E}-GFP) were sequenced by using the same protocol.

Western blot

About 0.8×10^6 cells were lysed by mixing with $100 \, \mu l$ of PBS, $100 \, \mu l$ of phenol (pH8.0), and $5 \, \mu l$ of β -mercaptoethanol, and vortexed for 15 min. Proteins were precipitated by mixing with $1.2 \, m l$ methanol containing 0.1 M ammonium acetate followed by centrifugation at $4 \, ^{\circ} C$ for 30 min. The proteins were resolved on sodium dodecyl sulphate polyacrylamide gel electrophoresis gels, transferred onto polyvinylidene difluoride membranes (Immobilon-P; Millipore) and probed with primary

(Supplementary Table S12) and secondary antibodies. Blots were incubated with SuperSignal West Femto Maximum Sensitivity Substrate (Thermo Scientific) and scanned by using a ChemiDocTM XRS + System (Bio-Rad).

Generation of $DBT^{-/-}$ melanocyte cell lines

Hermes 4C melanocytes were transduced with lentiviral particles packaged with sgDBT-mCherry as described above. Two weeks after the transduction, single cells were deposited into individual wells of 96-well plates containing conditioned medium (spent media harvested from cell cultures) by using FACS. Cells that had grown into clones were passaged periodically to expand the populations. Genomic DNA was isolated from the clones and sequenced across the Cas9 cutting site of the DBT gene by using the same strategy as described above. Clones with biallelic frameshift indels in the DBT gene (DBT^{-/-}) were further confirmed to be devoid of DBT protein by western blots.

Complementation of $DBT^{-\prime-}$ cells with DBT cDNA

DBT $^{-/-}$ cells were transduced with lentiviral particles packaged with EF–DBT–BSD (Supplementary Table S1). Three days after the transduction, blasticidin was added to the culture to a final concentration of $10\,\mu\text{g/ml}$ to eliminate the untransduced cells. Expression of the DBT protein was confirmed by Western blot.

Senescence-associated β-galactosidase assay

Hermes 4C melanocytes were transduced with lentiviral particles packaged with EF–BRAF V600E –GFP. Five to nine days later, the transduced and untransduced cells were stained with the β -Galactosidase Staining Kit (Cell Signaling, 9860) following the manufacture's instruction.

Apoptosis assay

About 10⁵ cells were transduced with lentiviral particles packaged with EF-BRAFV600E-Hyg or PGK-BRAFV600E-Hyg (Supplementary Table S1), giving rise to ~75% transduction efficiency. Three, six, and nine days after the transduction, cells were stained with fluorescein-conjugated Annexin V (Thermo Fisher Scientific) and analyzed by using flow cytometry.

KIC and HMB treatments

Cultures of Hermes 4C melanocytes were added with different concentrations of sodium 4-methyl-2-oxovalerate (KIC) (Sigma, K0629) and 3-hydroxy-3-methylbutyric acid (HMB) (Alfa Aesar, 42722-09). After 24 and 48 h of

incubation, whole-cell protein extracts were made and the levels of total and phosphorylated ERK1/2 were measured by western blot as described above.

Overexpression of DBT in melanoma cell lines

Melanoma cell lines were transduced with lentiviral particles packaged with EF-mCherry (as a control) or EF-DBT-mCherry (Supplementary Table S1), giving rise to >90% transduction efficiency. The medium was changed every 3 days after the transduction.

Mining of data in TCGA (The Cancer Genome Atlas) and GTEX (Genotype-Tissue Expression)

cBioPortal [31] was utilized to analyze GPR4 and DBT mutations in cancers based on the TCGA database [32]. GEPIA [33] was used to analyze expressions of GPR4 and DBT in 23 cancer types and their matched normal tissues in the TCGA database. The correlations of BRAF expression with GPR4 and DBT expressions in cancers and normal tissues collected in TCGA and GTEX, respectively, were analyzed by using Xena [34] and the UCSC Toil RNAseq Recompute Data Hub (https://xena.ucsc.edu/). RSEM expected counts were normalized with DESeq2 [log₂ (expected_count-deseq2 + 1)].

Acknowledgements We are deeply in debt to Elena Sviderskaya and Philip Goff at Wellcome Trust Functional Genomics Cell Bank for supplying human melanocyte and melanoma cell lines. We also thank Mary Price at the Cell Analysis Core Facility, Louisiana Cancer Research Center for flow cytometry analysis, cell sorting and single cell deposition, and Dr Luan Vu at our department for analysis and graphic preparation of flow cytometry data. This study was supported by the National Science Foundation (MCB-1615550 to SL).

Compliance with ethical standards

Conflict of interest The authors declare that they have no conflict of interest.

Publisher's note Springer Nature remains neutral with regard to jurisdictional claims in published maps and institutional affiliations.

References

- Lee EY, Muller WJ. Oncogenes and tumor suppressor genes. Cold Spring Harb Perspect Biol. 2010;2:a003236.
- Bansal R, Nikiforov MA. Pathways of oncogene-induced senescence in human melanocytic cells. Cell Cycle. 2010;9:2782–8.
- Kotsantis P, Petermann E, Boulton SJ. Mechanisms of oncogeneinduced replication stress: jigsaw falling into place. Cancer Discov. 2018;8:537–55.
- Labazi M, Phillips AC. Oncogenes as regulators of apoptosis. Essays Biochem. 2003;39:89–104.
- Lowe SW, Cepero E, Evan G. Intrinsic tumour suppression. Nature. 2004;432:307–15.

 McDuff FK, Turner SD. Jailbreak: oncogene-induced senescence and its evasion. Cell Signal. 2011;23:6–13.

- Shortt J, Johnstone RW. Oncogenes in cell survival and cell death. Cold Spring Harb Perspect Biol. 2012;4:a009829.
- Childs BG, Baker DJ, Kirkland JL, Campisi J, van Deursen JM. Senescence and apoptosis: dueling or complementary cell fates? EMBO Rep. 2014;15:1139–53.
- Hernandez B, Adissu HA, Wei BR, Michael HT, Merlino G, Simpson RM. Naturally occurring canine melanoma as a predictive comparative oncology model for human mucosal and other triple wild-type melanomas. Int J Mol Sci. 2018;19: pii: E394.
- Brennan DF, Dar AC, Hertz NT, Chao WC, Burlingame AL, Shokat KM, et al. A Raf-induced allosteric transition of KSR stimulates phosphorylation of MEK, Nature, 2011;472:366–9.
- Dankner M, Rose AAN, Rajkumar S, Siegel PM, Watson IR. Classifying BRAF alterations in cancer: new rational therapeutic strategies for actionable mutations. Oncogene. 2018;3183–99.
- 12. Davies H, Bignell GR, Cox C, Stephens P, Edkins S, Clegg S, et al. Mutations of the BRAF gene in human cancer. Nature. 2002;417:949–54.
- Kong BY, Carlino MS, Menzies AM. Biology and treatment of BRAF mutant metastatic melanoma. Melanoma Manag. 2016;3:33–45.
- Michaloglou C, Vredeveld LC, Soengas MS, Denoyelle C, Kuilman T, van der Horst CM, et al. BRAFE600-associated senescence-like cell cycle arrest of human naevi. Nature. 2005;436:720–4.
- Pollock PM, Harper UL, Hansen KS, Yudt LM, Stark M, Robbins CM, et al. High frequency of BRAF mutations in nevi. Nat Genet. 2003;33:19–20.
- Acosta JC, O'Loghlen A, Banito A, Guijarro MV, Augert A, Raguz S, et al. Chemokine signaling via the CXCR2 receptor reinforces senescence. Cell. 2008;133:1006–18.
- 17. Kuilman T, Michaloglou C, Vredeveld LC, Douma S, van Doorn R, Desmet CJ, et al. Oncogene-induced senescence relayed by an interleukin-dependent inflammatory network. Cell. 2008;133:1019–31.
- Vredeveld LC, Possik PA, Smit MA, Meissl K, Michaloglou C, Horlings HM, et al. Abrogation of BRAFV600E-induced senescence by PI3K pathway activation contributes to melanomagenesis. Genes Dev. 2012;26:1055–69.
- Gray-Schopfer VC, Cheong SC, Chong H, Chow J, Moss T, Abdel-Malek ZA, et al. Cellular senescence in naevi and immortalisation in melanoma: a role forp16? Br J Cancer. 2006;95:496–505.
- Scott MC, Wakamatsu K, Ito S, Kadekaro AL, Kobayashi N, Groden J, et al. Human melanocortin 1 receptor variants, receptor function and melanocyte response to UV radiation. J Cell Sci. 2002;115:2349–55.
- Chellappan S, Kraus VB, Kroger B, Munger K, Howley PM, Phelps WC, et al. Adenovirus-E1a, simian virus-40 tumorantigen, and human papillomavirus-E7 Protein share the capacity to disrupt the interaction between transcription factor-E2f and the retinoblastoma gene-product. P Natl Acad Sci USA. 1992;89:4549–53.
- Shamma A, Takegami Y, Miki T, Kitajima S, Noda M, Obara T, et al. Rb Regulates DNA damage response and cellular senescence through E2F-dependent suppression of N-ras isoprenylation. Cancer Cell. 2009;15:255–69.
- Hernandez-Segura A, Nehme J, Demaria M. Hallmarks of cellular senescence. Trends Cell Biol. 2018;28:436–53.
- Sanjana NE, Shalem O, Zhang F. Improved vectors and genome-wide libraries for CRISPR screening. Nat Methods. 2014;11:783–4.
- Li W, Xu H, Xiao T, Cong L, Love MI, Zhang F, et al. MAGeCK enables robust identification of essential genes from genome-scale CRISPR/Cas9 knockout screens. Genome Biol. 2014;15:554.

- Fukuda H, Ito S, Watari K, Mogi C, Arisawa M, Okajima F, et al. Identification of a potent and selective GPR4 antagonist as a drug lead for the treatment of myocardial infarction. ACS Med Chem Lett. 2016;7:493–7.
- Dong B, Zhang X, Fan Y, Cao S, Zhang X. GPR4 knockout improves renal ischemia-reperfusion injury and inhibits apoptosis via suppressing the expression of CHOP. Biochem J. 2017;474:4065–74.
- Castellone RD, Leffler NR, Dong L, Yang LV. Inhibition of tumor cell migration and metastasis by the proton-sensing GPR4 receptor. Cancer Lett. 2011;312:197–208.
- Surh CD, Danner DJ, Ahmed A, Coppel RL, Mackay IR, Dickson ER, et al. Reactivity of primary biliary cirrhosis sera with a human fetal liver cDNA clone of branched-chain alpha-keto acid dehydrogenase dihydrolipoamide acyltransferase, the 52 kD mitochondrial autoantigen. Hepatology. 1989;9:63–68.
- Tsuruta M, Mitsubuchi H, Mardy S, Miura Y, Hayashida Y, Kinugasa A, et al. Molecular basis of intermittent maple syrup urine disease: novel mutations in the E2 gene of the branchedchain alpha-keto acid dehydrogenase complex. J Hum Genet. 1998;43:91–100.
- 31. Cerami E, Gao J, Dogrusoz U, Gross BE, Sumer SO, Aksoy BA, et al. The cBio cancer genomics portal: an open platform for exploring multidimensional cancer genomics data. Cancer Discov. 2012;2:401–4.
- Tomczak K, Czerwinska P, Wiznerowicz M. The Cancer Genome Atlas (TCGA): an immeasurable source of knowledge. Contemp Oncol. 2015;19:A68–77.
- 33. Tang Z, Li C, Kang B, Gao G, Li C, Zhang Z. GEPIA: a web server for cancer and normal gene expression profiling and interactive analyses. Nucleic Acids Res. 2017;45:W98–W102.
- 34. Goldman M, Graft B, Hastie M, Repečka K, Kamath A, McDade F, et al. The UCSC Xena platform for public and private cancer genomics data visualization and interpretation. bioRxiv 2019.
- Melnikova VO, Santamaria AB, Bolshakov SV, Ananthaswamy HN. Mutant p53 is constitutively phosphorylated at Serine 15 in UV-induced mouse skin tumors: involvement of ERK1/2 MAP kinase. Oncogene. 2003;22:5958–66.
- She QB, Chen NY, Dong ZG. ERKs and p38 kinase phosphorylate p53 protein at serine 15 in response to UV radiation. J Biol Chem. 2000;275:20444–9.
- 37. Xirodimas D, Saville MK, Edling C, Lane DP, Lain S. Different effects of p14ARF on the levels of ubiquitinated p53 and Mdm2 in vivo. Oncogene. 2001;20:4972–83.
- 38. Palmero I, Pantoja C, Serrano M. p19ARF links the tumour suppressor p53 to Ras. Nature. 1998;395:125–6.
- Zindy F, Eischen CM, Randle DH, Kamijo T, Cleveland JL, Sherr CJ, et al. Myc signaling via the ARF tumor suppressor regulates p53-dependent apoptosis and immortalization. Genes Dev. 1998;12:2424–33.
- Ogawara Y, Kishishita S, Obata T, Isazawa Y, Suzuki T, Tanaka K, et al. Akt enhances Mdm2-mediated ubiquitination and degradation of p53. J Biol Chem. 2002;277:21843–50.
- 41. Gottlieb TM, Leal JF, Seger R, Taya Y, Oren M. Cross-talk between Akt, p53 and Mdm2: possible implications for the regulation of apoptosis. Oncogene. 2002;21:1299–303.
- 42. Georgakilas AG, Martin OA, Bonner WM. p21: A two-faced genome guardian. Trends Mol Med. 2017;23:310–9.
- 43. Galanos P, Vougas K, Walter D, Polyzos A, Maya-Mendoza A, Haagensen EJ, et al. Chronic p53-independent p21 expression causes genomic instability by deregulating replication licensing. Nat Cell Biol. 2016;18:777–89.

- 44. Kidger AM, Keyse SM. The regulation of oncogenic Ras/ERK signalling by dual-specificity mitogen activated protein kinase phosphatases (MKPs). Semin Cell Dev Biol. 2016;50:125–32.
- Lake D, Correa SA, Muller J. Negative feedback regulation of the ERK1/2 MAPK pathway. Cell Mol Life Sci. 2016;73:4397–413.
- Carpenter K. Branched chain amino acids and maple syrup urine disease. In: Rajendram R, Preedy VR, Patel V, editors. Branched chain amino acids in clinical nutrition, vol. 1. New York: Humana Press; 2015. p. 145–56.
- Cole JT. Metabolism of BCAAa. In: Rajendram R, Preedy VR, Patel V, editors. Branched chain amino acids in clinical nutrition, vol. 1. New York: Humana Press; 2015. p. 13–24.
- Blackburn PR, Gass JM, Vairo FPE, Farnham KM, Atwal HK, Macklin S, et al. Maple syrup urine disease: mechanisms and management. Appl Clin Genet. 2017;10:57–66.
- Holecek M. Branched-chain amino acids in health and disease: metabolism, alterations in blood plasma, and as supplements. Nutr Metab. 2018;15:33.
- Wellbrock C, Arozarena I. The complexity of the ERK/MAPkinase pathway and the treatment of melanoma skin cancer. Front Cell Dev Biol. 2016;4:33.
- Caloca MJ, Zugaza JL, Matallanas D, Crespo P, Bustelo XR. Vav mediates Ras stimulation by direct activation of the GDP/GTP exchange factor Ras GRP1. EMBO J. 2003;22:3326–36.
- 52. Costello PS, Walters AE, Mee PJ, Turner M, Reynolds LF, Prisco A, et al. TheRho-family GTP exchange factor Vav is a critical transducer of T cell receptor signals to the calcium, ERK, and NF-kappa B pathways. P Natl Acad Sci USA. 1999;96:3035–40.
- Reynolds LF, de Bettignies C, Norton T, Beeser A, Chernoff J, Tybulewicz VL. Vav1 transduces T cell receptor signals to the activation of the Ras/ERK pathway via LAT, Sos, and RasGRP1. J Biol Chem. 2004;279:18239–46.
- Wilsbacher JL, Moores SL, Brugge JS. An active form of Vav1 induces migration of mammary epithelial cells by stimulating secretion of an epidermal growth factor receptor ligand. Cell Commun Signal. 2006;4:5.
- Deschenes-Simard X, Gaumont-Leclerc MF, Bourdeau V, Lessard F, Moiseeva O, Forest V, et al. Tumor suppressor activity of the ERK/MAPK pathway by promoting selective protein degradation. Genes Dev. 2013;27:900–15.
- Sin WC, Zhang Y, Zhong W, Adhikarakunnathu S, Powers S, Hoey T, et al. G protein-coupled receptors GPR4 and TDAG8 are oncogenic and overexpressed in human cancers. Oncogene. 2004;23:6299–303.
- 57. Wyder L, Suply T, Ricoux B, Billy E, Schnell C, Baumgarten BU, et al. Reduced pathological angiogenesis and tumor growth in mice lacking GPR4, a proton sensing receptor. Angiogenesis. 2011;14:533–44.
- Dong L, Krewson EA, Yang LV. Acidosis activates endoplasmic reticulum stress pathways through gpr4 in human vascular endothelial cells. Int J Mol Sci. 2017;18:278.
- Bektas M, Barak LS, Jolly PS, Liu H, Lynch KR, Lacana E, et al. The G protein-coupled receptor GPR4 suppresses ERK activation in a ligand-independent manner. Biochemistry. 2003;42:12181–91.
- Brown JP, Wei WY, Sedivy JM. Bypass of senescence after disruption ofp21(CIP1/WAF1) gene in normal diploid human fibroblasts. Science. 1997;277:831–4.
- Bandyopadhyay D, Medrano EE. Melanin accumulation accelerates melanocyte senescence by a mechanism involvingp16(INK4a)/CDK4/pRB and E2F1. Mol Cell Gerontol. 2000;908:71–84.
- Dhanasekaran DN, Kashef K, Lee CM, Xu H, Reddy EP. Scaffold proteins of MAP-kinase modules. Oncogene. 2007;26:3185–202.

- 63. Hedman AC, Smith JM, Sacks DB. The biology of IQGAP proteins: beyond the cytoskeleton. Embo Rep. 2015;16:427–46.
- 64. Kakadia S, Yarlagadda N, Awad R, Kundranda M, Niu JX, Naraev B, et al. Mechanisms of resistance to BRAF and MEK inhibitors and clinical update of US Food and Drug Administration-approved targeted therapy in advanced melanoma. Oncotargets Ther. 2018;11:7095–107.
- Sambrook J, Russell DW. Calcium-phosphate-mediated transfection of eukaryotic cells with plasmid DNAs. CSH Protoc. 2006;2006: pii: pdb.prot3871.
- Li W, Koster J, Xu H, Chen CH, Xiao T, Liu JS, et al. Quality control, modeling, and visualization of CRISPR screens with MAGeCK-VISPR. Genome Biol. 2015;16:281.

Supplementary information for Ko et al "Genome-wide screening identifies novel genes implicated in cellular sensitivity to BRAF^{V600E} expression" (12 tables and 5 Figures).

Supplementary Table S1. Len	Supplementary Table S1. Lentiviral transfer vectors used in this study.				
Name	Encoded sgRNA	Encoded protein	Source		
lentiCRISPR v2	none (stuffer)	Cas9-P2A-puromycin	Addgene		
GeCKO libraries v2	libraries	Cas9-P2A-puromycin	Addgene		
EF-BRAFV600E-GFP	none	$BRAF^{V600E}$ - $P2A$ - GFP^c	this study		
PGK-BRAFV600E-GFP	none	$BRAF^{V600E}\text{-}P2A\text{-}GFP^d$	this study		
EF-GFP	none	GFP^e	this study		
EF-BRAFV600E-Hyg	none	BRAF ^{V600E} -P2A-hygromycin ^f	this study		
PGK-BRAFV600E-Hyg	none	BRAF ^{V600E} -P2A-hygromycin ^g	this study		
sgDBT-mCherry	DBT-targeting ^a	Cas9-P2A-mCherry ^h	this study		
sgGPR4-mCherry	GPR4-targeting ^b	Cas9-P2A-mCherry ^h	this study		
EF-DBT-BSD	none	DBT-P2A-blasticidin ⁱ	this study		
EF-DBT-mCherry	none	DBT-P2A-mCherry ^j	this study		
EF-mCherry	none	mCherry ^l	this study		

^a The DBT-targeting sgRNA sequence is GTCCATCATAACGACTAGTGA.

Supplementary Table S2. sgRNAs detected in Hermes 4C melanocytes survived BRAF ^{V600E} overexpression.					
Gene ^a	Control_count	BRAF ^{V600E} _count	Fold change	p-value	FDR
GPR4	396.7	1.18E+06	2976.5	0	0
DBT	158.8	2.96E+05	1866.6	0	0
SLC6A20	397.3	3.41E+05	858.1	0	0
LYPLA1	18.6	6301.7	338.5	0	0
OR8K1	26.2	3852.2	147.2	0	0
WNT4	30.8	4172.6	135.3	0	0
ZBTB40	21.5	2716.5	126.2	0	0
PHKA1	36.1	3838	106.4	0	0
TMEM43	41.3	4325.7	104.7	0	0
OR6B2	38.4	3072.5	80.0	0	0
SULT4A1	13.4	1014.7	75.8	0	0
KCNH8	40.1	2866	71.4	0	0
ZNF653	48.9	3421.4	70.0	0	0
TMEM107	60.5	3731.2	61.7	0	0
NPM1	52.4	2567	49.0	2.54E-308	4.05E-307
CELA3A	30.2	1249.7	41.3	2.37E-226	3.53E-222
TMEM256	4.1	145.97	35.8	3.63E-157	5.10E-153
VAV1	16.9	516.24	30.6	5.27E-123	7.00E-119
hsa-mir-4519	39.0	1182	30.3	1.40E-120	1.76E-116
ERK2 (MAPK1)	16.9	363.15	21.5	3.13E-60	3.74E-56
EGFL7	18.6	242.1	13.0	7.30E-22	8.31E-18
DCUN1D4	75.6	712.05	9.4	1.75E-11	1.90E-07
DPP3	19.8	181.57	9.2	4.56E-11	4.74E-07
NYAP2	37.2	320.42	8.6	9.05E-10	9.01E-06
DOCK5	42.5	323.98	7.6	8.63E-08	0.0008244

^b The GPR4-targeting sgRNA sequence is GCGCCGATGACAAAGATGTAG.

^c Driven by the EF1α promoter; the sequences of BRAF^{V600E} cDNA and GFP gene were from plasmids pBABE-Puro-BRAF-V600E (Addgene) and pmaxGFP (Lonza), respectively.

^d Same as in lenti-EF-BRAFV600E-GFP but the EF1α promoter replaced by the PGK promoter from plasmid pLJM1-EGFP (Addgene).

^e Same as in EF-BRAFV600E-GFP but the BRAFV600E and P2A sequences removed.

^fSame as in EF-BRAFV600E-GFP but the GFP sequence replaced by hygromycin sequence.

g Same as in PGK-BRAFV600E-GFP but the GFP replaced by hygromycin sequence.

^h The mCherry sequence was from plasmid pLM-CMV-R-Cre (Addgene).

ⁱ Driven by the EF1α promoter; the DBT cDNA was from Dharmacon (clone 3924492) with 3 silent mutations (Fig. 5A).

^j Same as in EF-DBT-BSD but the blasticidin sequence replaced by mCherry.

¹ Same as in EF-DBT-BSD but the DBT cDNA-P2A-blasticidin sequences replaced by mCherry.

NUDT17	43.0	306.18	7.1	7.47E-07	0.0068648
HEYL	12.8	81.886	6.4	1.14E-05	0.10121
FAM72B	3.5	17.801	5.1	0.0012081	0.10121
ZBTB37	46.5	181.57	3.9	0.0012081	0.27693
CHD9	21.5	81.886	3.8	0.015451	0.32157
hsa-mir-4670	27.3	99.688	3.6	0.010104	0.32157
MFSD11	27.3	96.127	3.5	0.022249	0.32157
RNF151	11.6	39.163	3.4	0.038449	0.32157
TNFSF4	24.4	81.886	3.4	0.038726	0.32157
SLC7A1	6.4	21.362	3.3	0.042992	0.32157
ATG4A	23.8	78.326	3.3	0.04368	0.32157
GPR179	25.0	81.886	3.3	0.044495	0.32157
MIA	4.7	14.241	3.1	0.071717	0.32157
YIPF6	23.8	71.205	3.0	0.072179	0.32157
ZNF610	30.8	7.1205	0.2	0.92731	0.32157
FOXK1	15.7	3.5603	0.2	0.92875	0.32157
ARFGAP1	16.3	3.5603	0.2	0.93144	0.32157
hsa-mir-3973	18.0	3.5603	0.2	0.93843	0.32157
TMEM97	19.2	3.5603	0.2	0.94236	0.32157
DHRS4L2	20.4	3.5603	0.2	0.94581	0.32157
CGN	44.8	7.1205	0.2	0.95098	0.32157
MAPK15	23.3	3.5603	0.2	0.95288	0.32157
PKD1L3	24.4	3.5603	0.1	0.95522	0.32157
NOTCH3	25.0	3.5603	0.1	0.9563	0.32157
hsa-mir-6839	26.2	3.5603	0.1	0.95832	0.32157
HTR1E	26.2	3.5603	0.1	0.95832	0.32157
STAC3	27.3	3.5603	0.1	0.96017	0.32157
TEKT1	27.9	3.5603	0.1	0.96103	0.32157
KCTD9	28.5	3.5603	0.1	0.96185	0.32157
hsa-mir-4720	40.7	3.5603	0.1	0.9736	0.32157
ECHDC1	54.7	3.5603	0.1	0.98048	0.32157
hsa-mir-2114	12.2	35.603	2.9	0.081715	0.32212
LRWD1	13.4	3.5603	0.3	0.91549	0.32212
HOXA9	12.2	3.5603	0.3	0.90684	0.32545
GSR	23.3	7.1205	0.3	0.90173	0.32917
ZNF77	22.1	7.1205	0.3	0.89613	0.33392
RPS6KL1	16.9	46.284	2.7	0.10487	0.33713
DENND4B	9.3	3.5603	0.4	0.87507	0.35095
UBAC2	18.6	7.1205	0.4	0.87479	0.35173
SERPINB10	9.9	24.922	2.5	0.14573	0.38194
KDM8	23.8	10.681	0.4	0.85112	0.39019
hsa-mir-6748	7.6	3.5603	0.5	0.84336	0.39747
TUBB3	41.9	99.688	2.4	0.17316	0.42586
GTPBP1	6.4	3.5603	0.6	0.81191	0.44903
CHTOP	12.2	7.1205	0.6	0.8008	0.47555
HRC	11.1	24.922	2.3	0.2034	0.48475
ST8SIA5	11.6	7.1205	0.6	0.7897	0.48818
GCSAML	6.4	14.241	2.2	0.21559	0.50045
SIGLEC9	27.3	17.801	0.7	0.77425	0.52401
STX3	7.0	14.241	2.0	0.26442	0.58756
TPP1	4.7	3.5603	0.8	0.73339	0.58756
DDX24	1.7	3.5603	2.0	0.30362	0.65294
MAP2K6	18.6	32.042	1.7	0.35927	0.7535
ANKRD13D	31.4	53.404	1.7	0.36666	0.76027
SEMG1	17.5	28.482	1.6	0.39051	0.80972
CENPB	16.3	17.801	1.1	0.59787	0.8338
STMN3	6.4	7.1205	1.1	0.59366	0.84252
CDKN1A	37.2	42.723	1.1	0.57601	0.87911
OR4C12	21.5	24.922	1.2	0.57156	0.88832
MPDU1	4.7	7.1205	1.5	0.43756	0.89289
CLEC12B	17.5	24.922	1.4	0.46577	0.93157
SFRP5	16.9	21.362	1.3	0.52863	0.94276

WFIKKN2	14.0	17.801	1.3	0.52552	0.94897
XPNPEP2	14.0	17.801	1.3	0.52552	0.94897
C18orf54	23.8	32.042	1.3	0.49816	0.99632

a shown in bold are genes whose targeting sgRNAs were also significantly enriched in BRAFV600E-overexpressing P1F/TERT fibroblasts; shown in red are genes known to be implicated in cancers; shown in gray are genes whose targeting sgRNAs were detected but not significantly enriched [false discovery rate (FDR) > 0.1].

Gene ^a	Control_count	BRAF ^{V600E} _count	Fold change	p-value	FDR
DR8K1	20.0	3.58E+05	17916	0	0
OR6B2	21.2	2.81E+05	13277	0	0
CNH8	28.6	2.59E+05	9048	0	0
ZBTB40	29.2	2.56E+05	8797	0	0
PHKA1	46.9	3.53E+05	7531	0	0
NF653	60.6	3.20E+05	5288	0	0
VAV1	19.4	48456.0	2493	0	0
CGFL7	14.9	25862.0	1740	0	0
CRK2 (MAPK1)	22.3	32815.0	1472	0	0
MEM256	9.7	13933.0	1434	0	0
IEYL	8.6	7962.3	929	0	0
OCK5	37.7	31326.0	830	0	0
TG4A	14.3	8269.6	579	0	0
UDT17	66.3	31993.0	482	0	0
sa-mir-4670	17.1	8165.8	476	0	0
EBTB37	41.7	18243.0	437	0	0
YAP2	63.4	24873.0	392	0	0
⁄IΙΑ	5.7	2175.2	381	0	0
PP3	46.3	15214.0	329	0	0
TPF6	27.4	6657.2	243	0	0
NFSF4	33.2	7204.0	217	0	0
SPR179	47.4	9530.8	201	0	0
ERPINB10	14.9	2913.5	196	0	0
EMG1	13.7	2670.1	195	0	0
IRC	17.1	3192.9	186	0	0
VFIKKN2	18.9	3101.1	164	0	0
C18orf54	13.7	1983.6	145	0	0
AM72B	9.1	1305.1	143	0	0
TX3	9.1	1297.1	142	0	0
PS6KL1	32.6	4537.9	139	0	0
DDX24	5.1	670.5	130	0	0
sa-mir-2114	23.4	2913.5	124	0	0
FRP5	15.4	1604.4	104	0	0
NF151	32.0	3316.6	104	0	0
CLEC12B	33.2	3097.1	93	0	0
CDKN1A	38.9	3456.3	89	0	0
MAP2K6	38.9	3105.1	80	0	0
OR4C12	30.9	2127.3	69	0	0
CENPB	21.2	1349.0	64	0	0
NKRD13D	57.7	3180.9	55	0	0
MPDU1	7.4	319.3	43	1.17E-232	6.83E-229
MFSD11	60.6	2410.6	40	8.52E-202	4.85E-198
TPBP1	16.0	451.0	28	4.06E-101	4.85E-198 2.26E-97
RRC56	10.3	287.4	28	2.02E-98	2.20E-97 1.10E-94
PP1	5.7	159.6	28	1.82E-95	9.67E-92
IGLEC9	50.3	1325.0	26	1.82E-93 1.12E-87	5.83E-84
KPNPEP2	12.6	327.3	26	9.96E-86	5.06E-82

GCNT7	11.4	291.4	25	5.59E-82	2.78E-78
DENND4B	9.1	223.5	24	9.31E-75	4.54E-71
PKD1L3	46.9	1065.6	23	4.14E-65	1.98E-61
CHTOP	16.6	359.2	22	2.25E-59	1.05E-55
TEKT1	49.7	1037.7	21	1.11E-54	5.12E-51
UBAC2	17.1	347.2	20	8.96E-52	4.04E-48
ZNF77	51.4	1005.8	20	6.67E-48	2.95E-44
DHRS4L2	29.2	502.9	17	1.85E-37	8.05E-34
MAP3K4	4.6	79.8	17	3.31E-36	1.41E-32
SLC22A17	1.7	31.9	19	5.03E-35	2.11E-31
ZNF506	14.3	187.6	13	1.23E-21	5.07E-18
SCLT1	32.6	399.1	12	6.91E-19	2.80E-15
ARFGAP1	30.3	359.2	12	1.01E-17	4.03E-14
ZNF22	4.0	47.9	12	7.21E-17	2.83E-13
FBLN7	6.3	71.8	11	5.50E-16	2.12E-12
OR51Q1	22.9	251.4	11	2.63E-15	9.98E-12
KDM8	38.9	403.1	10	1.31E-13	4.91E-10
hsa-mir-6748	12.0	115.7	10	8.51E-12	3.13E-08
ZNF610	35.4	323.3	9	1.21E-10	4.38E-07
GOLGA6B	10.9	95.8	9	6.24E-10	2.22E-06
SELL	18.9	155.7	8	7.91E-09	2.78E-05
PEX7	23.4	187.6	8	2.42E-08	8.37E-05
GSR	40.0	299.3	7	2.42E-07	0.0008267
hsa-mir-346	19.4	139.7	7	7.53E-07	0.0025344
NOTCH3	21.7	155.7	7	8.18E-07	0.0027148
STMN3	14.9	103.8	7	1.72E-06	0.0056453
COL11A2	42.9	299.3	7	1.78E-06	0.0057437
VIPAS39	27.4	187.6	7	2.93E-06	0.0093407
MRRF	5.1	35.9	7	2.98E-06	0.0093407
SCG5	3.4	23.9	7	4.89E-06	0.0053088
					0.01.210
KRTAP6-2	22.3	135.7	6	4.12E-05	0.061559
KRTAP6-2 CD6	22.3 10.9	135.7 63.9	6 6	4.12E-05 8.70E-05	0.061559 0.061559
KRTAP6-2 CD6 Mapk15	22.3 10.9 66.9	135.7 63.9 391.1	6 6 6	4.12E-05 8.70E-05 9.88E-05	0.061559 0.061559 0.061559
KRTAP6-2 CD6 MAPK15 CGN	22.3 10.9 66.9 31.4	135.7 63.9 391.1 179.6	6 6 6	4.12E-05 8.70E-05 9.88E-05 0.00013858	0.061559 0.061559 0.061559 0.061559
KRTAP6-2 CD6 MAPK15 CGN GPR4	22.3 10.9 66.9 31.4 89.7	135.7 63.9 391.1 179.6 463.0	6 6 6 6 5	4.12E-05 8.70E-05 9.88E-05 0.00013858 0.00077663	0.061559 0.061559 0.061559 0.061559 0.087691
KRTAP6-2 CD6 MAPK15 CGN GPR4 ANKRD10	22.3 10.9 66.9 31.4 89.7 6.3	135.7 63.9 391.1 179.6 463.0 31.9	6 6 6 6 5 5	4.12E-05 8.70E-05 9.88E-05 0.00013858 0.00077663 0.0010572	0.061559 0.061559 0.061559 0.061559 0.087691 0.11932
KRTAP6-2 CD6 MAPK15 CGN GPR4 ANKRD10 STAC3	22.3 10.9 66.9 31.4 89.7 6.3 32.6	135.7 63.9 391.1 179.6 463.0 31.9 151.7	6 6 6 5 5 5	4.12E-05 8.70E-05 9.88E-05 0.00013858 0.00077663 0.0010572 0.0026397	0.061559 0.061559 0.061559 0.061559 0.087691 0.11932 0.29749
KRTAP6-2 CD6 MAPK15 CGN GPR4 ANKRD10	22.3 10.9 66.9 31.4 89.7 6.3 32.6 30.3	135.7 63.9 391.1 179.6 463.0 31.9 151.7 131.7	6 6 6 6 5 5	4.12E-05 8.70E-05 9.88E-05 0.00013858 0.00077663 0.0010572	0.061559 0.061559 0.061559 0.061559 0.087691 0.11932 0.29749 0.31572
KRTAP6-2 CD6 MAPK15 CGN GPR4 ANKRD10 STAC3	22.3 10.9 66.9 31.4 89.7 6.3 32.6	135.7 63.9 391.1 179.6 463.0 31.9 151.7	6 6 6 5 5 5	4.12E-05 8.70E-05 9.88E-05 0.00013858 0.00077663 0.0010572 0.0026397	0.061559 0.061559 0.061559 0.061559 0.087691 0.11932 0.29749
KRTAP6-2 CD6 MAPK15 CGN GPR4 ANKRD10 STAC3 SLC46A1	22.3 10.9 66.9 31.4 89.7 6.3 32.6 30.3	135.7 63.9 391.1 179.6 463.0 31.9 151.7 131.7	6 6 6 5 5 5	4.12E-05 8.70E-05 9.88E-05 0.00013858 0.00077663 0.0010572 0.0026397 0.0054931	0.061559 0.061559 0.061559 0.061559 0.087691 0.11932 0.29749 0.31572
KRTAP6-2 CD6 MAPK15 CGN GPR4 ANKRD10 STAC3 SLC46A1 HOXC13	22.3 10.9 66.9 31.4 89.7 6.3 32.6 30.3 8.6	135.7 63.9 391.1 179.6 463.0 31.9 151.7 131.7	6 6 6 5 5 5 4 4	4.12E-05 8.70E-05 9.88E-05 0.00013858 0.00077663 0.0010572 0.0026397 0.0054931 0.02173	0.061559 0.061559 0.061559 0.061559 0.087691 0.11932 0.29749 0.31572
KRTAP6-2 CD6 MAPK15 CGN GPR4 ANKRD10 STAC3 SLC46A1 HOXC13 CYP1A1	22.3 10.9 66.9 31.4 89.7 6.3 32.6 30.3 8.6 20.6	135.7 63.9 391.1 179.6 463.0 31.9 151.7 131.7 31.9 71.8	6 6 6 5 5 5 4 4 3	4.12E-05 8.70E-05 9.88E-05 0.00013858 0.00077663 0.0010572 0.0026397 0.0054931 0.02173 0.032165	0.061559 0.061559 0.061559 0.061559 0.087691 0.11932 0.29749 0.31572 0.31572
KRTAP6-2 CD6 MAPK15 CGN GPR4 ANKRD10 STAC3 SLC46A1 HOXC13 CYP1A1 FOXK1	22.3 10.9 66.9 31.4 89.7 6.3 32.6 30.3 8.6 20.6 65.2	135.7 63.9 391.1 179.6 463.0 31.9 151.7 131.7 31.9 71.8 227.5	6 6 6 5 5 5 4 4 4 3 3	4.12E-05 8.70E-05 9.88E-05 0.00013858 0.00077663 0.0010572 0.0026397 0.0054931 0.02173 0.032165 0.033126	0.061559 0.061559 0.061559 0.061559 0.087691 0.11932 0.29749 0.31572 0.31572 0.31572
KRTAP6-2 CD6 MAPK15 CGN GPR4 ANKRD10 STAC3 SLC46A1 HOXC13 CYP1A1 FOXK1 ZFHX2	22.3 10.9 66.9 31.4 89.7 6.3 32.6 30.3 8.6 20.6 65.2 4.6 6.3	135.7 63.9 391.1 179.6 463.0 31.9 151.7 131.7 31.9 71.8 227.5 16.0	6 6 6 5 5 5 4 4 3 3	4.12E-05 8.70E-05 9.88E-05 0.00013858 0.00077663 0.0010572 0.0026397 0.0054931 0.02173 0.032165 0.033126 0.037239	0.061559 0.061559 0.061559 0.061559 0.087691 0.11932 0.29749 0.31572 0.31572 0.31572 0.31572
KRTAP6-2 CD6 MAPK15 CGN GPR4 ANKRD10 STAC3 SLC46A1 HOXC13 CYP1A1 FOXK1 ZFHX2 CXorf30 TMEM154	22.3 10.9 66.9 31.4 89.7 6.3 32.6 30.3 8.6 20.6 65.2 4.6 6.3 16.6	135.7 63.9 391.1 179.6 463.0 31.9 151.7 131.7 31.9 71.8 227.5 16.0 20.0 51.9	6 6 6 5 5 5 4 4 3 3 3	4.12E-05 8.70E-05 9.88E-05 0.00013858 0.00077663 0.0010572 0.0026397 0.0054931 0.02173 0.032165 0.033126 0.037239 0.059906 0.060342	0.061559 0.061559 0.061559 0.061559 0.087691 0.11932 0.29749 0.31572 0.31572 0.31572 0.31572 0.31572 0.31572 0.31572
KRTAP6-2 CD6 MAPK15 CGN GPR4 ANKRD10 STAC3 SLC46A1 HOXC13 CYP1A1 FOXK1 ZFHX2 CXorf30 TMEM154 CCNT2	22.3 10.9 66.9 31.4 89.7 6.3 32.6 30.3 8.6 20.6 65.2 4.6 6.3 16.6 88.0	135.7 63.9 391.1 179.6 463.0 31.9 151.7 131.7 31.9 71.8 227.5 16.0 20.0 51.9 20.0	6 6 6 5 5 5 4 4 4 3 3 3 3	4.12E-05 8.70E-05 9.88E-05 0.00013858 0.00077663 0.0010572 0.0026397 0.0054931 0.02173 0.032165 0.033126 0.037239 0.059906 0.060342 0.92909	0.061559 0.061559 0.061559 0.061559 0.087691 0.11932 0.29749 0.31572 0.31572 0.31572 0.31572 0.31572 0.31572 0.31572 0.31572
KRTAP6-2 CD6 MAPK15 CGN GPR4 ANKRD10 STAC3 SLC46A1 HOXC13 CYP1A1 FOXK1 ZFHX2 CXorf30 TMEM154 CCNT2 EIF4A1	22.3 10.9 66.9 31.4 89.7 6.3 32.6 30.3 8.6 20.6 65.2 4.6 6.3 16.6 88.0 21.2	135.7 63.9 391.1 179.6 463.0 31.9 151.7 131.7 31.9 71.8 227.5 16.0 20.0 51.9 20.0 4.0	6 6 6 5 5 5 4 4 3 3 3 3 3 0 0	4.12E-05 8.70E-05 9.88E-05 0.00013858 0.00077663 0.0010572 0.0026397 0.0054931 0.02173 0.032165 0.033126 0.037239 0.059906 0.060342 0.92909 0.94146	0.061559 0.061559 0.061559 0.061559 0.087691 0.11932 0.29749 0.31572 0.31572 0.31572 0.31572 0.31572 0.31572 0.31572 0.31572 0.31572
KRTAP6-2 CD6 MAPK15 CGN GPR4 ANKRD10 STAC3 SLC46A1 HOXC13 CYP1A1 FOXK1 ZFHX2 CXorf30 TMEM154 CCNT2 EIF4A1 MFSD8	22.3 10.9 66.9 31.4 89.7 6.3 32.6 30.3 8.6 20.6 65.2 4.6 6.3 16.6 88.0 21.2 86.3	135.7 63.9 391.1 179.6 463.0 31.9 151.7 131.7 31.9 71.8 227.5 16.0 20.0 51.9 20.0 4.0 16.0	6 6 6 5 5 5 4 4 4 3 3 3 3 3 0 0	4.12E-05 8.70E-05 9.88E-05 0.00013858 0.00077663 0.0010572 0.0026397 0.0054931 0.02173 0.032165 0.033126 0.037239 0.059906 0.060342 0.92909 0.94146 0.94278	0.061559 0.061559 0.061559 0.061559 0.087691 0.11932 0.29749 0.31572 0.31572 0.31572 0.31572 0.31572 0.31572 0.31572 0.31572 0.31572 0.31572 0.31572
KRTAP6-2 CD6 MAPK15 CGN GPR4 ANKRD10 STAC3 SLC46A1 HOXC13 CYP1A1 FOXK1 ZFHX2 CXorf30 TMEM154 CCNT2 EIF4A1 MFSD8 ESYT3	22.3 10.9 66.9 31.4 89.7 6.3 32.6 30.3 8.6 20.6 65.2 4.6 6.3 16.6 88.0 21.2 86.3 21.7	135.7 63.9 391.1 179.6 463.0 31.9 151.7 131.7 31.9 71.8 227.5 16.0 20.0 51.9 20.0 4.0 16.0 4.0	6 6 6 5 5 5 4 4 4 3 3 3 3 3 0 0 0	4.12E-05 8.70E-05 9.88E-05 0.00013858 0.00077663 0.0010572 0.0026397 0.0054931 0.02173 0.032165 0.033126 0.037239 0.059906 0.060342 0.92909 0.94146 0.94278 0.94308	0.061559 0.061559 0.061559 0.061559 0.087691 0.11932 0.29749 0.31572 0.31572 0.31572 0.31572 0.31572 0.31572 0.31572 0.31572 0.31572 0.31572 0.31572 0.31572
KRTAP6-2 CD6 MAPK15 CGN GPR4 ANKRD10 STAC3 SLC46A1 HOXC13 CYP1A1 FOXK1 ZFHX2 CXorf30 TMEM154 CCNT2 EIF4A1 MFSD8 ESYT3 SDE2	22.3 10.9 66.9 31.4 89.7 6.3 32.6 30.3 8.6 20.6 65.2 4.6 6.3 16.6 88.0 21.2 86.3 21.7 22.3	135.7 63.9 391.1 179.6 463.0 31.9 151.7 131.7 31.9 71.8 227.5 16.0 20.0 51.9 20.0 4.0 16.0 4.0	6 6 6 5 5 5 5 4 4 4 3 3 3 3 3 0 0 0	4.12E-05 8.70E-05 9.88E-05 0.00013858 0.00077663 0.0010572 0.0026397 0.0054931 0.02173 0.032165 0.037239 0.059906 0.060342 0.92909 0.94146 0.94278 0.94308 0.94461	0.061559 0.061559 0.061559 0.061559 0.087691 0.11932 0.29749 0.31572 0.31572 0.31572 0.31572 0.31572 0.31572 0.31572 0.31572 0.31572 0.31572 0.31572 0.31572 0.31572
KRTAP6-2 CD6 MAPK15 CGN GPR4 ANKRD10 STAC3 SLC46A1 HOXC13 CYP1A1 FOXK1 ZFHX2 CXorf30 TMEM154 CCNT2 EIF4A1 MFSD8 ESYT3 SDE2 hsa-mir-6716	22.3 10.9 66.9 31.4 89.7 6.3 32.6 30.3 8.6 20.6 65.2 4.6 6.3 16.6 88.0 21.2 86.3 21.7 22.3 22.9	135.7 63.9 391.1 179.6 463.0 31.9 151.7 131.7 31.9 71.8 227.5 16.0 20.0 51.9 20.0 4.0 4.0 4.0	6 6 6 5 5 5 4 4 4 3 3 3 3 3 0 0 0 0	4.12E-05 8.70E-05 9.88E-05 0.00013858 0.00077663 0.0010572 0.0026397 0.0054931 0.02173 0.032165 0.037239 0.059906 0.060342 0.92909 0.94146 0.94278 0.94308 0.94461 0.94606	0.061559 0.061559 0.061559 0.061559 0.087691 0.11932 0.29749 0.31572 0.31572 0.31572 0.31572 0.31572 0.31572 0.31572 0.31572 0.31572 0.31572 0.31572 0.31572 0.31572 0.31572
KRTAP6-2 CD6 MAPK15 CGN GPR4 ANKRD10 STAC3 SLC46A1 HOXC13 CYP1A1 FOXK1 ZFHX2 CXorf30 TMEM154 CCNT2 EIF4A1 MFSD8 ESYT3 SDE2 hsa-mir-6716 GMPR	22.3 10.9 66.9 31.4 89.7 6.3 32.6 30.3 8.6 20.6 65.2 4.6 6.3 16.6 88.0 21.2 86.3 21.7 22.3 22.9 52.6	135.7 63.9 391.1 179.6 463.0 31.9 151.7 131.7 31.9 71.8 227.5 16.0 20.0 51.9 20.0 4.0 4.0 4.0 4.0	6 6 6 5 5 5 4 4 4 3 3 3 3 3 0 0 0 0 0	4.12E-05 8.70E-05 9.88E-05 0.00013858 0.00077663 0.0010572 0.0026397 0.0054931 0.02173 0.032165 0.033126 0.037239 0.059906 0.060342 0.92909 0.94146 0.94278 0.94308 0.94461 0.94606 0.95343	0.061559 0.061559 0.061559 0.061559 0.087691 0.11932 0.29749 0.31572 0.31572 0.31572 0.31572 0.31572 0.31572 0.31572 0.31572 0.31572 0.31572 0.31572 0.31572 0.31572 0.31572 0.31572
KRTAP6-2 CD6 MAPK15 CGN GPR4 ANKRD10 STAC3 SLC46A1 HOXC13 CYP1A1 FOXK1 ZFHX2 CXorf30 TMEM154 CCNT2 EIF4A1 MFSD8 ESYT3 SDE2 hsa-mir-6716 GMPR C16orf52	22.3 10.9 66.9 31.4 89.7 6.3 32.6 30.3 8.6 20.6 65.2 4.6 6.3 16.6 88.0 21.2 86.3 21.7 22.3 22.9 52.6 53.7	135.7 63.9 391.1 179.6 463.0 31.9 151.7 131.7 31.9 71.8 227.5 16.0 20.0 51.9 20.0 4.0 16.0 4.0 4.0 4.0 8.0 8.0	6 6 6 5 5 5 4 4 4 3 3 3 3 3 0 0 0 0 0	4.12E-05 8.70E-05 9.88E-05 0.00013858 0.00077663 0.0010572 0.0026397 0.0054931 0.02173 0.032165 0.033126 0.037239 0.059906 0.060342 0.92909 0.94146 0.94278 0.94308 0.94461 0.94606 0.95343 0.95446	0.061559 0.061559 0.061559 0.061559 0.087691 0.11932 0.29749 0.31572 0.31572 0.31572 0.31572 0.31572 0.31572 0.31572 0.31572 0.31572 0.31572 0.31572 0.31572 0.31572 0.31572 0.31572 0.31572 0.31572
KRTAP6-2 CD6 MAPK15 CGN GPR4 ANKRD10 STAC3 SLC46A1 HOXC13 CYP1A1 FOXK1 ZFHX2 CXorf30 TMEM154 CCNT2 EIF4A1 MFSD8 ESYT3 SDE2 hsa-mir-6716 GMPR C16orf52 THBS2	22.3 10.9 66.9 31.4 89.7 6.3 32.6 30.3 8.6 20.6 65.2 4.6 6.3 16.6 88.0 21.2 86.3 21.7 22.3 22.9 52.6 53.7 58.9	135.7 63.9 391.1 179.6 463.0 31.9 151.7 131.7 31.9 71.8 227.5 16.0 20.0 51.9 20.0 4.0 16.0 4.0 4.0 4.0 8.0 8.0 8.0	6 6 6 5 5 5 4 4 4 3 3 3 3 3 0 0 0 0 0 0	4.12E-05 8.70E-05 9.88E-05 0.00013858 0.00077663 0.0010572 0.0026397 0.0054931 0.02173 0.032165 0.033126 0.037239 0.059906 0.060342 0.92909 0.94146 0.94278 0.94308 0.94461 0.94606 0.95343 0.9586	0.061559 0.061559 0.061559 0.061559 0.087691 0.11932 0.29749 0.31572 0.31572 0.31572 0.31572 0.31572 0.31572 0.31572 0.31572 0.31572 0.31572 0.31572 0.31572 0.31572 0.31572 0.31572 0.31572 0.31572 0.31572
KRTAP6-2 CD6 MAPK15 CGN GPR4 ANKRD10 STAC3 SLC46A1 HOXC13 CYP1A1 FOXK1 ZFHX2 CXorf30 TMEM154 CCNT2 EIF4A1 MFSD8 ESYT3 SDE2 hsa-mir-6716 GMPR C16orf52 THBS2 ASAH2B	22.3 10.9 66.9 31.4 89.7 6.3 32.6 30.3 8.6 20.6 65.2 4.6 6.3 16.6 88.0 21.2 86.3 21.7 22.3 22.9 52.6 53.7 58.9 29.7	135.7 63.9 391.1 179.6 463.0 31.9 151.7 131.7 31.9 71.8 227.5 16.0 20.0 51.9 20.0 4.0 16.0 4.0 4.0 4.0 8.0 8.0 8.0 8.0 8.0 8.0	6 6 6 5 5 5 4 4 4 3 3 3 3 3 0 0 0 0 0 0 0	4.12E-05 8.70E-05 9.88E-05 0.00013858 0.00077663 0.0010572 0.0026397 0.0054931 0.02173 0.032165 0.037239 0.059906 0.060342 0.92909 0.94146 0.94278 0.94308 0.94461 0.94606 0.95343 0.95446 0.9586 0.95898	0.061559 0.061559 0.061559 0.061559 0.087691 0.11932 0.29749 0.31572
KRTAP6-2 CD6 MAPK15 CGN GPR4 ANKRD10 STAC3 SLC46A1 HOXC13 CYP1A1 FOXK1 ZFHX2 CXorf30 TMEM154 CCNT2 EIF4A1 MFSD8 ESYT3 SDE2 hsa-mir-6716 GMPR C16orf52 THBS2 ASAH2B KIF1B	22.3 10.9 66.9 31.4 89.7 6.3 32.6 30.3 8.6 20.6 65.2 4.6 6.3 16.6 88.0 21.2 86.3 21.7 22.3 22.9 52.6 53.7 58.9 29.7 31.4	135.7 63.9 391.1 179.6 463.0 31.9 151.7 131.7 31.9 71.8 227.5 16.0 20.0 51.9 20.0 4.0 16.0 4.0 4.0 4.0 4.0 4.0 4.0 4.0 8.0 8.0 8.0 8.0 8.0 8.0 8.0 8.0	6 6 6 5 5 5 5 4 4 4 3 3 3 3 3 0 0 0 0 0 0 0 0 0	4.12E-05 8.70E-05 9.88E-05 0.00013858 0.00077663 0.0010572 0.0026397 0.0054931 0.02173 0.032165 0.037239 0.059906 0.060342 0.92909 0.94146 0.94278 0.94308 0.94461 0.94606 0.95343 0.9586 0.95886 0.95898 0.9613	0.061559 0.061559 0.061559 0.061559 0.087691 0.11932 0.29749 0.31572
KRTAP6-2 CD6 MAPK15 CGN GPR4 ANKRD10 STAC3 SLC46A1 HOXC13 CYP1A1 FOXK1 ZFHX2 CXorf30 TMEM154 CCNT2 EIF4A1 MFSD8 ESYT3 SDE2 hsa-mir-6716 GMPR C16orf52 THBS2 ASAH2B KIF1B CORO7	22.3 10.9 66.9 31.4 89.7 6.3 32.6 30.3 8.6 20.6 65.2 4.6 6.3 16.6 88.0 21.2 86.3 21.7 22.3 22.9 52.6 53.7 58.9 29.7 31.4 34.3	135.7 63.9 391.1 179.6 463.0 31.9 151.7 131.7 31.9 71.8 227.5 16.0 20.0 51.9 20.0 4.0 16.0 4.0 4.0 4.0 4.0 4.0 4.0 4.0 4.0 8.0 8.0 8.0 8.0 8.0 8.0 8.0 4.0 4.0 4.0	6 6 6 5 5 5 5 4 4 4 3 3 3 3 3 0 0 0 0 0 0 0 0 0 0 0	4.12E-05 8.70E-05 9.88E-05 0.00013858 0.00077663 0.0010572 0.0026397 0.0054931 0.02173 0.032165 0.037239 0.059906 0.060342 0.92909 0.94146 0.94278 0.94308 0.94461 0.94606 0.95343 0.95898 0.95898 0.9613 0.96463	0.061559 0.061559 0.061559 0.061559 0.087691 0.11932 0.29749 0.31572
KRTAP6-2 CD6 MAPK15 CGN GPR4 ANKRD10 STAC3 SLC46A1 HOXC13 CYP1A1 FOXK1 ZFHX2 CXorf30 TMEM154 CCNT2 EIF4A1 MFSD8 ESYT3 SDE2 hsa-mir-6716 GMPR C16orf52 THBS2 ASAH2B KIF1B CORO7 ATM	22.3 10.9 66.9 31.4 89.7 6.3 32.6 30.3 8.6 20.6 65.2 4.6 6.3 16.6 88.0 21.2 86.3 21.7 22.3 22.9 52.6 53.7 58.9 29.7 31.4 34.3 35.4	135.7 63.9 391.1 179.6 463.0 31.9 151.7 131.7 31.9 71.8 227.5 16.0 20.0 51.9 20.0 4.0 16.0 4.0 4.0 4.0 4.0 4.0 4.0 4.0 4.0 4.0 8.0 8.0 8.0 8.0 8.0 8.0 4.0 4.0 4.0 4.0	6 6 6 5 5 5 5 4 4 4 3 3 3 3 3 3 0 0 0 0 0 0 0 0 0 0 0	4.12E-05 8.70E-05 9.88E-05 0.00013858 0.00077663 0.0010572 0.0026397 0.0054931 0.02173 0.032165 0.037239 0.059906 0.060342 0.92909 0.94146 0.94278 0.94308 0.94461 0.94606 0.95343 0.9586 0.95886 0.95898 0.9613 0.96463 0.96581	0.061559 0.061559 0.061559 0.061559 0.061559 0.087691 0.11932 0.29749 0.31572
KRTAP6-2 CD6 MAPK15 CGN GPR4 ANKRD10 STAC3 SLC46A1 HOXC13 CYP1A1 FOXK1 ZFHX2 CXorf30 TMEM154 CCNT2 EIF4A1 MFSD8 ESYT3 SDE2 hsa-mir-6716 GMPR C16orf52 THBS2 ASAH2B KIF1B CORO7	22.3 10.9 66.9 31.4 89.7 6.3 32.6 30.3 8.6 20.6 65.2 4.6 6.3 16.6 88.0 21.2 86.3 21.7 22.3 22.9 52.6 53.7 58.9 29.7 31.4 34.3	135.7 63.9 391.1 179.6 463.0 31.9 151.7 131.7 31.9 71.8 227.5 16.0 20.0 51.9 20.0 4.0 16.0 4.0 4.0 4.0 4.0 4.0 4.0 4.0 4.0 8.0 8.0 8.0 8.0 8.0 8.0 8.0 4.0 4.0 4.0	6 6 6 5 5 5 5 4 4 4 3 3 3 3 3 0 0 0 0 0 0 0 0 0 0 0	4.12E-05 8.70E-05 9.88E-05 0.00013858 0.00077663 0.0010572 0.0026397 0.0054931 0.02173 0.032165 0.037239 0.059906 0.060342 0.92909 0.94146 0.94278 0.94308 0.94461 0.94606 0.95343 0.95898 0.95898 0.9613 0.96463	0.061559 0.061559 0.061559 0.061559 0.087691 0.11932 0.29749 0.31572

OD 5311/1	26.0	4.0	0	0.06627	0.21572
OR52W1	36.0	4.0	0	0.96637	0.31572
STAU1	46.3	4.0	0	0.97404	0.31572
SUPT4H1	50.3	4.0	0	0.97615	0.31572
TMEM107	89.2	4.0	0	0.98669	0.31572
KRTAP7-1	32.6	8.0	0	0.92286	0.31633
hsa-mir-3973	25.7	75.8	3	0.08044	0.317
ARRB2	15.4	4.0	0	0.91828	0.317
FCRL6	31.4	8.0	0	0.91986	0.317
MYO15A	99.5	27.9	0	0.91094	0.32161
SLC22A2	13.7	4.0	0	0.90732	0.32321
RBMY1A1	181.8	59.9	0	0.89455	0.33778
LOC100130357	18.9	51.9	3	0.10797	0.34091
STK19	46.3	16.0	0	0.88872	0.34496
CFI	33.2	12.0	0	0.88292	0.35293
ODF1	21.7	8.0	0	0.88064	0.35341
URB2	62.3	167.6	3	0.11937	0.35345
TXNDC16	28.6	75.8	3	0.12399	0.3625
hsa-mir-4720	31.4	12.0	0	0.87594	0.3625
UGT2A1	61.2	23.9	0	0.87233	0.36618
RNF2	48.6	20.0	0	0.86539	0.37423
SPNS2	19.4	8.0	0	0.86525	0.37463
PDE8A	18.9	8.0	0	0.86077	0.38707
ATP2A1	10.9	27.9	3	0.13986	0.38766
ATP2B2	9.1	4.0	0	0.85634	0.38766
hsa-mir-7855	46.3	20.0	0	0.85808	0.38766
ZFP91	36.0	16.0	0	0.85354	0.39521
ETV7	20.6	51.9	3	0.1481	0.39321
			3		
ZIK1	57.2	143.7		0.1513	0.40419
SEZ6L2	17.1	8.0	0	0.84541	0.40535
MEFV	19.4	47.9	2	0.1596	0.41848
TUBGCP2	40.0	20.0	0	0.83328	0.42495
ZFP106	29.7	16.0	1	0.81892	0.44888
DHCR24	36.6	20.0	1	0.81585	0.4565
VSTM2A	43.4	23.9	1	0.81377	0.46163
ADAMTS5	8.6	20.0	2	0.19279	0.47498
ECHDC1	65.2	43.9	1	0.76746	0.53921
PASD1	29.7	20.0	1	0.76782	0.53921
IL23A	29.2	20.0	1	0.76272	0.54207
N4BP3	22.9	47.9	2	0.24874	0.56082
CDIP1	10.9	8.0	1	0.74355	0.57819
AKT1	19.4	39.9	2	0.26028	0.58682
LRWD1	19.4	39.9	2	0.26028	0.58682
RPL26L1	19.4	39.9	2	0.26028	0.58682
HOXA9	25.7	51.9	2	0.27078	0.5962
GPBP1L1	29.7	23.9	1	0.71532	0.62679
FPR2	54.3	43.9	1	0.71472	0.6281
DBT	72.0	139.7	2	0.29645	0.65269
KCTD9	47.4	39.9	1	0.70163	0.65691
TRPV4	32.6	27.9	1	0.69485	0.66061
ZYG11B	86.9	163.6	2	0.31452	0.67753
hsa-mir-6839	28.0	51.9	2	0.32111	0.69173
SPIC	8.6	16.0	2	0.3211	0.69173
CAB39L	57.2	51.9	1	0.67551	0.69898
FLRT2	8.6	8.0	1	0.66692	0.09898
			1		
CDK20	17.1	16.0	1	0.66552	0.7205
HFE SNY12	4.0	4.0	1	0.64604	0.74677
SNX12	4.0	4.0	1	0.64604	0.74677
SOX11	28.6	27.9	1	0.64693	0.74677

ABCF1	8.0	8.0	1	0.64082	0.75776
LCE3D	35.4	35.9	1	0.63271	0.77487
MACROD1	27.4	27.9	1	0.63063	0.77925
CRNN	19.4	20.0	1	0.62717	0.78654
LRRC19	18.9	31.9	2	0.37414	0.78929
OR2V1	30.9	51.9	2	0.37839	0.79826
SLC24A3	11.4	12.0	1	0.61972	0.80001
HTR1E	22.3	23.9	1	0.60822	0.81301
CCDC71	10.9	12.0	1	0.59794	0.83434
MCM2	14.9	23.9	2	0.40303	0.83633
DNAH9	52.6	59.9	1	0.58359	0.84797
RNF32	20.6	31.9	2	0.4241	0.86362
TXLNG	20.6	31.9	2	0.4241	0.86362
OR4M1	16.6	20.0	1	0.55689	0.90233
DEFB114	42.3	51.9	1	0.54839	0.91963
INHA	10.9	16.0	1	0.45561	0.92777
SECISBP2	28.0	35.9	1	0.52598	0.96523
TUBAL3	36.6	51.9	1	0.47411	0.96541
SLC6A20	117.2	151.7	1	0.52461	0.96801
PDS5B	25.7	35.9	1	0.48197	0.98141
CHSY3	34.3	47.9	1	0.48228	0.98204
MICALL1	45.7	63.9	1	0.48282	0.98312
hsa-mir-6830	11.4	16.0	1	0.48305	0.98359
TMEM67	24.0	31.9	1	0.50745	0.99991

^a shown in bold are genes whose targeting sgRNAs were also significantly enriched in BRAF^{V600E}-overexpressing Hermes 4C melanocytes; shown in red are genes known to be implicated in cancers; shown in gray are genes whose targeting sgRNAs were detected but not significantly enriched [false discovery rate (FDR) > 0.1].

Supplementary Table S4. Distribution of GPR4 indels in single Hermes 4C melanocytes survived $BRAF^{V600E}$ overexpression.

Allele 1 ^a	Allele 2 ^a	Gene disruption ^b	Number of cells
(-10) 9 del, 4 ins	(-7) 6 del, 1 ins	biallelic	41
(-6) 16 del	large del	biallelic	8
(-6) 5 del	(-5) 5 del	biallelic	5
(-21) 43 del	large del	biallelic	4
(-2) 26 ins	large del	biallelic	2
(-2) 26 ins	(-7) 9 del, 4 ins	biallelic	1
(-2) 2 del	large del	biallelic	1
(-21) 43 del	(-6) 5 del	biallelic	1
(-5) 5 del	(-5) 6 del, 1 ins	biallelic	1
(-6) 16 del	(-6) 5 del	biallelic	1
(-64) 123 del	large del	biallelic	1
(-7) 6 del, 1 ins	(-6) 5 del	biallelic	1
(-5) 6 del	large del	monoallelic	1
		Total	68

[&]quot;Numbers in parentheses indicate start sites of insertions (ins) and/or deletions (del) (indels) relative to the CRISPR/Cas9 cutting site (Fig. 3B); numbers outside of parentheses indicate indel sizes (nucleotide numbers); a large del has > 200 nucleotides missing.

b an allele with a large del is considered disrupted.

Supplementary Table S5. Distribution of DBT indels in single Hermes 4C melanocytes survived BRAF ^{V600E} overexpression.			
Allele 1 ^a	Allele 2 ^a	Gene disruption ^b	Number of cells
(-1) 1 del	(+1) 2 del	biallelic	38
(+1) 2 del	large del	biallelic	37
(-1) 1 del	large del	biallelic	13
(-1) 10 del	(-1) 1 del	biallelic	2
(-1) 10 del	(+1) 4 ins	biallelic	1
(-1) 13 del	large del	biallelic	1
(-11) 11 del	large del	biallelic	1
(-11) 11 del	(-8) 15 del	monoallelic	1
		Total	94

^a Numbers in parentheses indicate start sites of insertions (ins) and/or deletions (del) (indels) relative to the CRISPR/Cas9 cutting site (Fig. 3C); numbers outside of parentheses indicate indel sizes (nucleotide numbers); a large del has > 200 nucleotides missing. ^b an allele with a large del is considered disrupted.

Supplementary Table S6. Distribution of GPR4 indels in single Hermes 4C melanocytes without BRAF ^{V600E} expression.			
Allele 1 ^a	Allele 2 ^a	Gene disruption ^b	Number of cells
(-1) 1 del	large del	biallelic	1
(-13) 31 del	(-3) 19 del	biallelic	1
(-27) 26 del	large del	biallelic	1
(-3) 2 del	(-1) 10 del	biallelic	1
(-1) 6 ins	large del	monoallelic	1
(-27) 26 del	(-4) 3 del	monoallelic	1
(-27) 26 del	(-5) 6 del	monoallelic	1
(-4) 3 del	large del	monoallelic	1
(-7) 6 del	(-5) 6 del	none	1
		Total	9

^a Numbers in parentheses indicate start sites of insertions (ins) and/or deletions (del) (indels) relative to the CRISPR/Cas9 cutting site (Fig. 3B); numbers outside of parentheses indicate indel sizes (nucleotide numbers); a large del has > 200 nucleotides missing.

^b an allele with a large del is considered to be disrupted.

Supplementary Table S7. Distribution of DBT indels in single Hermes 4C melanocytes without BRAF ^{V600E} expression.			
Allele 1 ^a	Allele 2 ^a	Gene disruption ^b	Number of cells
(-2) 3 del	(-1) 1 ins	monoallelic	3
(-2) 1 del	(-1) 2 del	biallelic	2
(-10) 11 del	(-2) 7 ins	biallelic	1
(-119) 118 del	(-2) 1 del	biallelic	1
(-2) 1 del	large del	biallelic	1
(-2) 3 del	large del	monoallelic	1
(-24) 33 del	large del	monoallelic	1
(-34) 123 del	(-10) 10 del	monoallelic	1
(-5) 6 del	(-2) 1 del	monoallelic	1
(-5) 6 del	(-3) 5 del	monoallelic	1
(-5) 6 del	(-4) 4 del	monoallelic	1
(-8) 6 del	(-1) 1 del	monoallelic	1
		Total	15

^a Numbers in parentheses indicate start sites of insertions (ins) and/or deletions (del) (indels) relative to the CRISPR/Cas9 cutting site (Fig. 3C); numbers outside of parentheses indicate indel sizes (nucleotide numbers); a large del has > 200 nucleotides missing. ^b an allele with a large del is considered to be disrupted.

Used XENA TCGA TARGET GTEx

Supplementary Table S8. Correlations of the expression level of BRAF with those of GPR4 and DBT in normal tissues (Spearman's rank rho)^a.

(Spearman S ганк гио).	Number of samples	BRAF vs GPR4	BRAF vs DBT
GTEX Adipose Tissue	512	0.05417	-0.01342
GTEX Adrenal Gland	126	0.1385	-0.1439
GTEX Bladder	9	0	-0.4167
GTEX Blood	941 ₄	-0.4472	-0.4505
GTEX Blood Vessel	604	-0.1883	0.215
GTEX Brain	1137	-0.4243	-0.2762
GTEX Breast	178	-0.00486	-0.2094
GTEX Cervix Uteri	10	-0.2848	-0.2848
GTEX Colon	307	0.283	0.3915
GTEX Esophagus	652	0.4014	0.07179
GTEX Fallopian Tube	5	-0.1	0.1
GTEX Heart	376	0.2117	-0.3673
GTEX Kidney	28	0.3304	0.06543
GTEX Liver	110	-0.01197	0.2083
GTEX Lung	288	0.4665	-0.3664
GTEX Muscle	395	0.2089	-0.00824
GTEX Nerve	278	-0.05791	0.1338
GTEX Ovary	88	0.1017	0.05068
GTEX Pancreas	167	0.1079	0.1393
GTEX Pituitary	107	0.04654	-0.1622
GTEX Prostate	100	0.05268	0.01877
GTEX Salivary Gland	55	0.008731	-0.01914
GTEX Skin	555	-0.03564	0.1632
GTEX Small Intestine	92	0.1407	0.2671
GTEX Spleen	100	0.1217	0.4433
GTEX Stomach	174	0.2072	0.1191
GTEX Testis	165	-0.02664	-0.5167
GTEX Thyroid	279	0.1138	-0.1374
GTEX Uterus	78	0.1189	-0.2368
GTEX Vagina	85	0.04213	-0.06236

^a The RNA-Seq data of GTEX (Genotype-Tissue Expression) were analyzed through the UCSC TOIL RNAseq Recompute Data Hub by using Xena (https://xena.ucsc.edu/). RSEM expected counts normalized with DESeq2 were used for the expression analyses.

Used XENA TCGA TARGET GTEx data

Supplementary Table S9. Correlations of the expression level of BRAF with those of GPR4 and DBT in cancers (Spearman's rank rho)^a.

	Number of samples	BRAF vs GPR4	BRAF vs DBT
TCGA Acute Myeloid Leukemia	173	-0.00035	0.5987
TCGA Adrenocortical Cancer	77	0.4149	0.4166
TCGA Bladder Urothelial Carcinoma	407	0.1754	0.6203
TCGA Brain Lower Grade Glioma	523	0.06156	0.455
TCGA Breast Invasive Carcinoma	1099	0.1366	0.4366
TCGA Cervical & Endocervical Cancer	306	0.2369	0.4825
TCGA Cholangiocarcinoma	36	0.3749	0.5013
TCGA Colon Adenocarcinoma	209	0.3733	0.4882
TCGA Diffuse Large B-Cell Lymphoma	47	0.2268	0.8066
TCGA Esophageal Carcinoma	182	0.3235	0.4329
TCGA Glioblastoma Multiforme	166	0.2951	0.567
TCGA Head & Neck Squamous Cell Carcinoma	520	0.3777	0.4952
TCGA Kidney Chromophobe	66	0.3417	0.2201
TCGA Kidney Clear Cell Carcinoma	531	0.2558	0.4527
TCGA Kidney Papillary Cell Carcinoma	289	0.1832	0.4674
TCGA Liver Hepatocellular Carcinoma	371	0.2556	0.3325

TCGA Lung Adenocarcinoma	515	0.1964	0.4054	
TCGA Lung Squamous Cell Carcinoma	498	0.2898	0.3576	
TCGA Mesothelioma	87	0.3983	0.5436	
TCGA Ovarian Serous Cystadenocarcinoma	427	0.2953	0.5362	
TCGA Pancreatic Adenocarcinoma	179	0.08013	0.4622	
TCGA Pheochromocytoma & Paraganglioma	182	0.3374	0.4891	
TCGA Prostate Adenocarcinoma	496	0.1729	0.3723	
TCGA Rectum Adenocarcinoma	93	0.4415	0.5353	
TCGA Sarcoma	319	0.1929	0.5218	
TCGA Skin Cutaneous Melanoma	469	-0.00035	0.5987	
TCGA Stomach Adenocarcinoma	414	0.092	0.3607	
TCGA Testicular Germ Cell Tumor	154	0.4326	0.2568	
TCGA Thymoma	119	0.3663	0.903	
TCGA Thyroid Carcinoma	512	0.07795	0.4901	
TCGA Uterine Carcinosarcoma	57	0.296	0.6119	
TCGA Uterine Corpus Endometrioid Carcinoma	181	0.2801	0.6309	
TCGA Uveal Melanoma	79	-0.2615	0.7888	

^a The RNA-Seq data of TCGA (The Cancer Genome Atlas) were analyzed through the UCSC TOIL RNAseq Recompute Data Hub by using Xena (https://xena.ucsc.edu/). RSEM expected counts normalized with DESeq2 were used for the expression analyses.

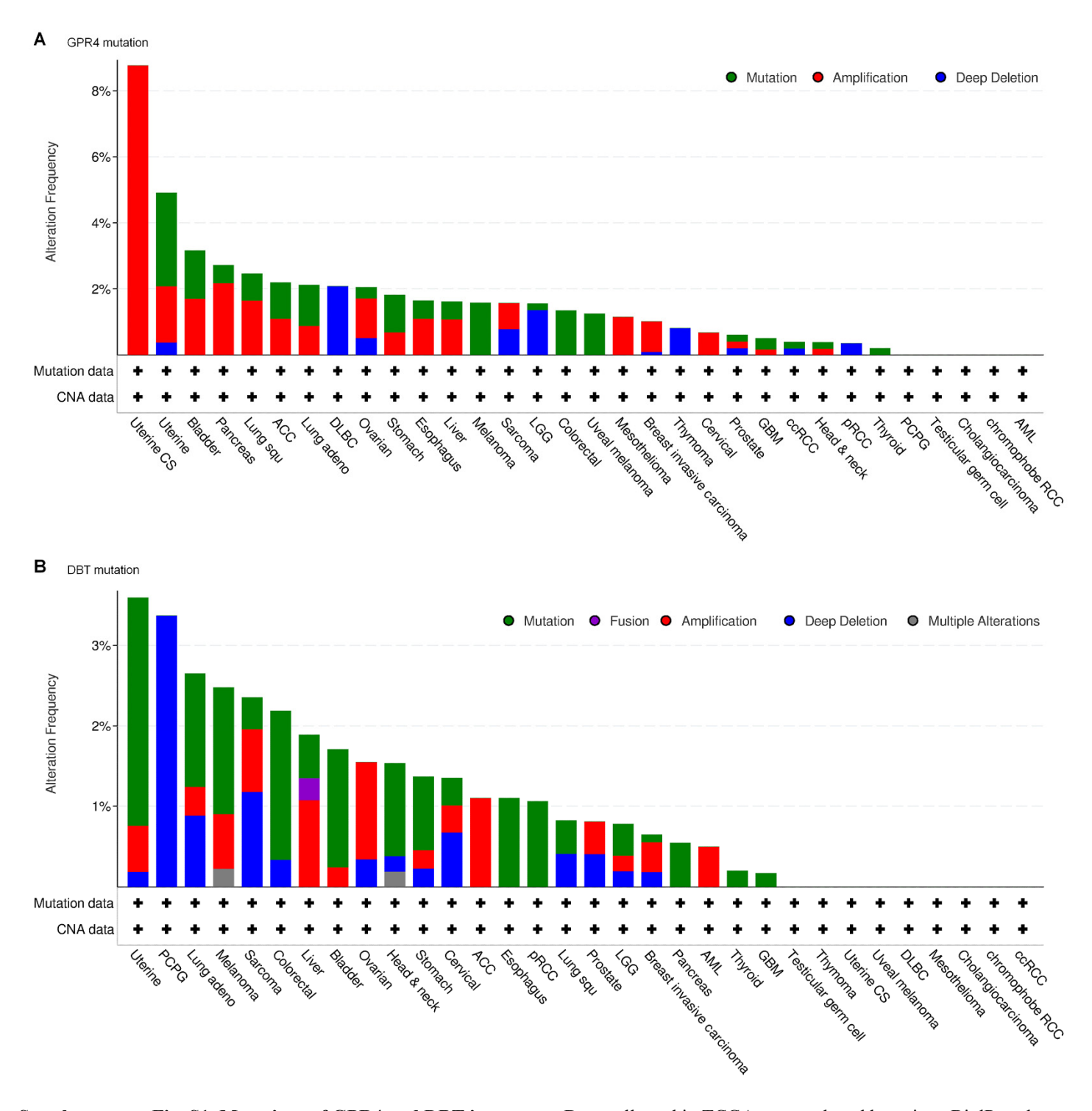
Supplementary Table S10. Primers used for amplification and sequencing of sgRNA-encoding sequences integrated into the genome of cells used.

Primer	Sequence ^a
Lenti-F1	ATGGACTATCATATGCTTACCGTAACTTGAAAGTATTTCG
Lenti-R1	ACTTCTTGTCCATGGTGGCAGC
GeCKO-1	ACACGACGCTCTTCCGATCTTCTTGTGGAAAGGACGAAACACCG
GeCKO-2	AGACGTGTGCTCTTCCGATCTACTTCTTGTCCATGGTGGCAGC
Tru-U	AATGATACGGCGACCACCGAGATCTACACTCTTTCCCTACACGACGCTCTTCCGATCT
Tru-B1	CAAGCAGAAGACGGCATACGAGAT <mark>CGTGAT</mark> GTGACTGGAGTTCAGACGTGTGCTCTTCCGATCT
Tru-B2	CAAGCAGAAGACGCATACGAGAT <mark>ACATCG</mark> GTGACTGGAGTTCAGACGTGTGCTCTTCCGATCT
Tru-B3	CAAGCAGAAGACGCCATACGAGAT <mark>GCCTAA</mark> GTGACTGGAGTTCAGACGTGTGCTCTTCCGATCT
Tru-B4	CAAGCAGAAGACGGCATACGAGAT <mark>TGGTCA</mark> GTGACTGGAGTTCAGACGTGTGCTCTTCCGATCT
1ru-B4	CAAGCAGAAGACGGCATACGAGATTGGTCAGTGACTGGACTTCAGACGTGTGCTCTTCCGATCT

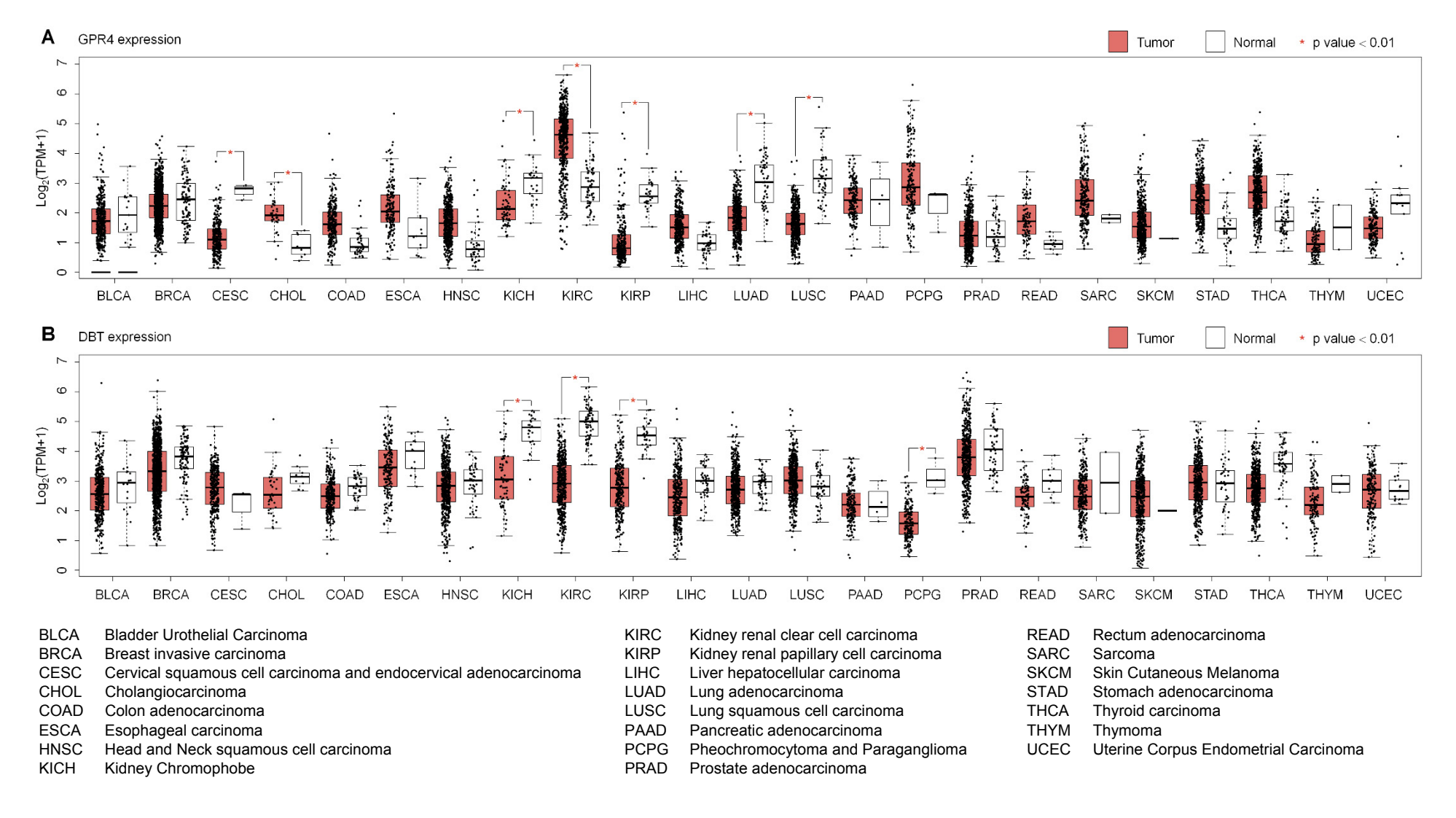
^a Shown in red are index (barcode) sequences used for next generation sequencing.

Primer	Table S11. Primers used for amplification and next-generation sequencing of DBT and GPR4 indels.
	Sequence ^a
DBT-F2	GAAGAAAGACTGGGAGAACTCCCATC
DBT-R2	CCTTTTCAATTTTCCTGATTTCGGCTTC
GPR4-F2	GCTACACATACTTCCTAATTGCCCTGC
GPR4-R2	GGTACGACAGCATGAGC
DBT-Tru-U	ACACGACGCTCTTCCGATCTGTACACCATCTGAAAGTAAATGCTGGG
DBT-Tru-Seq	AGACGTGTGCTCTTCCGATCTACGTTGAAAAGATTACATTTCCTCAAGAGC
GPR4-Tru-U	ACACGACGCTCTTCCGATCTTCTCTTCCCTGTAGACCACATCCC
GPR4-Tru-Seq	AGACGTGTGCTCTTCCGATCTCTGATGTAGATATTGGTGTAGAAGATGAACCC
Tru-U1	AATGATACGGCGACCACCGAGATCTACACCTCTCTATACACTCTTTCCCTACACGACGCTCTTCCGATCT
Tru-U2	AATGATACGGCGACCACCGAGATCTACACTATCCTCTACACTCTTTCCCTACACGACGCTCTTCCGATCT
Tru-U3	AATGATACGGCGACCACCGAGATCTACACGTAAGGAGACACTCTTTCCCTACACGACGCTCTTCCGATCT
Tru-U4	AATGATACGGCGACCACCGAGATCTACACACTGCATAACACTCTTTCCCTACACGACGCTCTTCCGATCT
Tru-U5	AATGATACGGCGACCACCGAGATCTACACAAGGAGTAACACTCTTTCCCTACACGACGCTCTTCCGATCT
Tru-U6	AATGATACGGCGACCACCGAGATCTACACCTAAGCCTACACTCTTTCCCTACACGACGCTCTTCCGATCT
Tru-U7	AATGATACGGCGACCACCGAGATCTACAC <mark>CGTCTAAT</mark> ACACTCTTTCCCTACACGACGCTCTTCCGATCT
Tru-U8	AATGATACGGCGACCACCGAGATCTACACTCTCTCCGACACTCTTTCCCTACACGACGCTCTTCCGATCT
Tru-B1	CAAGCAGAAGACGGCATACGAGAT <mark>CGTGAT</mark> GTGACTGGAGTTCAGACGTGTGCTCTTCCGATCT
Tru-B2	CAAGCAGAAGACGCATACGAGAT <mark>ACATCG</mark> GTGACTGGAGTTCAGACGTGTGCTCTTCCGATCT
Tru-B3	CAAGCAGAAGACGGCATACGAGAT <mark>GCCTAA</mark> GTGACTGGAGTTCAGACGTGTGCTCTTCCGATCT
Tru-B4	CAAGCAGAAGACGCATACGAGAT <mark>TGGTCA</mark> GTGACTGGAGTTCAGACGTGTGCTCTTCCGATCT
Tru-B5	CAAGCAGAAGACGGCATACGAGAT <mark>CACTGT</mark> GTGACTGGAGTTCAGACGTGTGCTCTTCCGATCT
Tru-B6	CAAGCAGAAGACGGCATACGAGAT <mark>ATTGGC</mark> GTGACTGGAGTTCAGACGTGTGCTCTTCCGATCT
Tru-B7	CAAGCAGAAGACGGCATACGAGAT <mark>GATCTG</mark> GTGACTGGAGTTCAGACGTGTGCTCTTCCGATCT
Tru-B8	CAAGCAGAAGACGGCATACGAGAT <mark>TCAAGT</mark> GTGACTGGAGTTCAGACGTGTGCTCTTCCGATCT
Tru-B9	CAAGCAGAAGACGGCATACGAGAT <mark>CTGATC</mark> GTGACTGGAGTTCAGACGTGTGCTCTTCCGATCT
Tru-B10	CAAGCAGAAGACGGCATACGAGAT <mark>AAGCTA</mark> GTGACTGGAGTTCAGACGTGTGCTCTTCCGATCT
Tru-B11	CAAGCAGAAGACGGCATACGAGAT <mark>GTAGCC</mark> GTGACTGGAGTTCAGACGTGTGCTCTTCCGATCT
Tru-B12	CAAGCAGAAGACGGCATACGAGAT <mark>TACAAG</mark> GTGACTGGAGTTCAGACGTGTGCTCTTCCGATCT
	e index (barcode) sequences used for next generation sequencing.

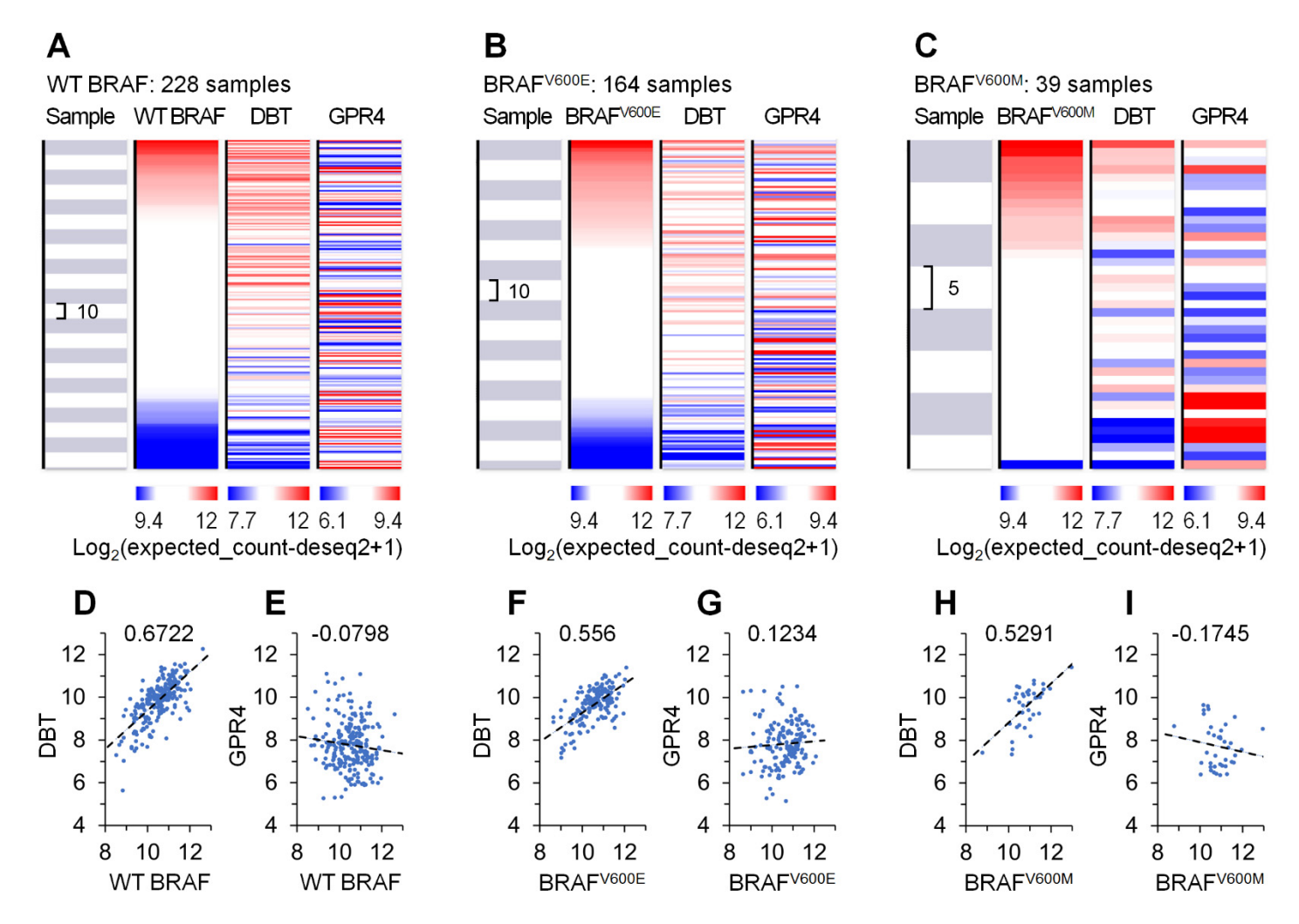
Supplementary Table S12. Primary antibodies used in this study.		
Protein recognized	Supplier (Cat. #)	
β-actin	Santa Cruz (sc-47778)	
AKT1	Santa Cruz (sc-55523)	
BRAF	Santa Cruz (sc-5284)	
DBT	Proteintech (12451-1-AP)	
DUSP4	Santa Cruz (sc-17821)	
DUSP5	Santa Cruz (sc-393801)	
DUSP6	Santa Cruz (sc-377070)	
ERK 1/2	Cell Signaling (9012)	
phosphorylated ERK1/2	Santa Cruz (sc-7383)	
GAPDH	Santa Cruz (sc-47724)	
MEK	Cell Signaling (4694)	
phosphorylated MEK	Cell Signaling (9121)	
p14 ^{ARF}	Santa Cruz (sc-53639)	
p15 ^{INK4b}	Santa Cruz (sc-271791)	
p16 ^{INK4a}	R&D Systems (AF5779)	
p21	Santa Cruz (sc-6246)	
p53	Santa Cruz (sc-126)	
Serine 15 phosphorylated p53	Cell Signaling (9284)	
Rb	Santa Cruz (sc-102)	



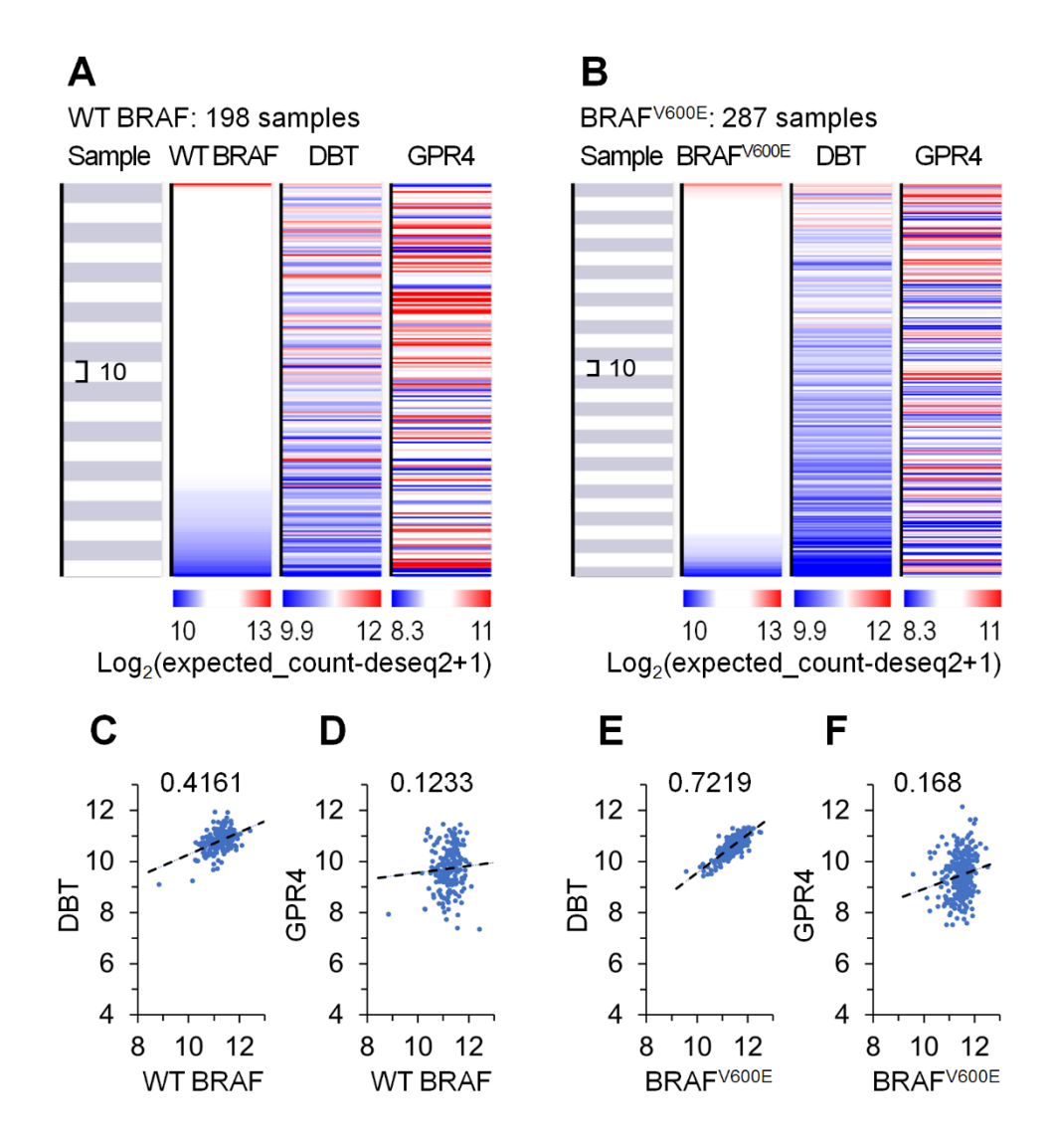
Supplementary Fig. S1. Mutations of GPR4 and DBT in cancers. Data collected in TCGA was analyzed by using cBiolPortal.



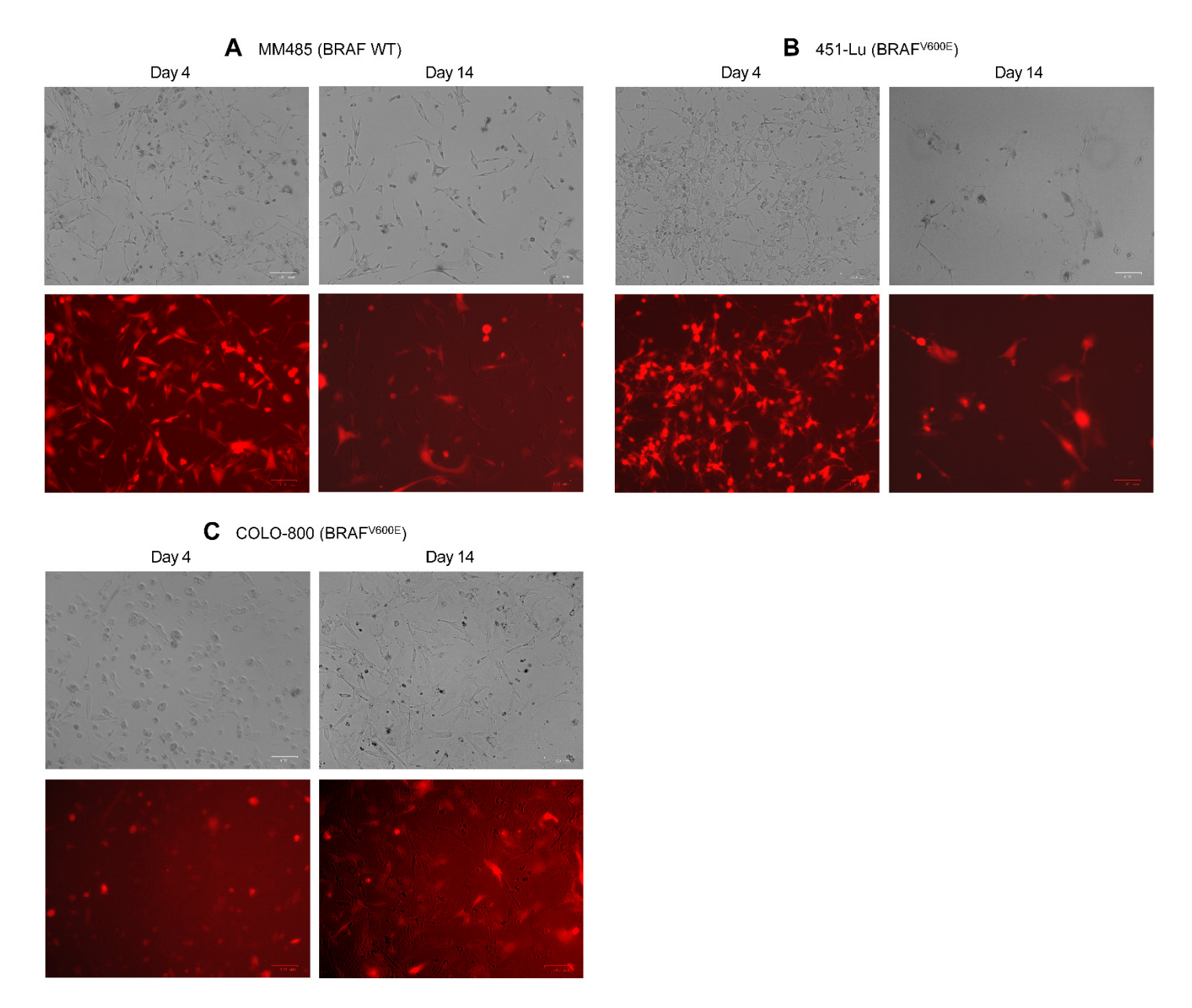
Supplementary Fig. S2. EPIA analysis of DBT and GPR4 mRNA levels in cancers and matched normal tissues. The analysis was based on RNA-Seq data collected in TCGA. Note that cancer types with no data of matched normal tissues are not included.



Supplementary Fig. S3. Expressions of BRAF, wild type and BRAF^{V600E} and BRAF^{V600M} mutants, are positively correlated with that of DBT, but not necessarily with that of GPR4, in skin cutaneous melanomas. (A-C) Visual spreadsheet showing expression levels of BRAF, DBT and GPR4 (sorted from high to low for the expression levels of BRAF) in skin cutaneous melanoma samples with wild type (WT) BRAF (A), BRAF^{V600E} (B) and BRAF^{V600M} (C). (D-I) Scatter plots showing correlations of BRAF expression with DBT and GPR4 expressions in skin cutaneous melanoma samples with WT BRAF, BRAF^{V600E} and BRAF^{V600M}. The expression levels are shown as RSEM expected counts normalized with DESeq2 [log₂(expected_count-deseq2+1)]. Numbers above plots are Spearman's rank rho values, which in the rages of 0.1 to 0.39, 0.4 to 0.69 and 0.7 to 1.0 are considered to be weak, moderate and strong positive correlations, respectively, and those of -0.1 to -0.39, -0.4 to -0.69 and -0.7 to -1.0 to be weak, moderate and strong negative correlations, respectively. The RNA-Seq data of TCGA (The Cancer Genome Atlas) skin cutaneous melanoma was analyzed through the UCSC TOIL RNAseq Recompute Data Hub on UCSC Xena (https://xena.ucsc.edu/).



Supplementary Fig. S4. Expressions of BRAF, wild type and the BRAF^{V600E} mutant, are positively correlated with those of DBT and GPR4 in thyroid carcinomas. (A and B) Visual spreadsheet showing expression levels of BRAF, DBT and GPR4 (sorted from high to low for the expression levels of BRAF) in thyroid carcinoma samples with wild type (WT) BRAF (A) and BRAF^{V600E} (B). (C-F) Scatter plots showing correlations of BRAF expression with DBT and GPR4 expressions in thyroid carcinoma samples with WT BRAF and BRAF^{V600E}. The expression levels are shown as RSEM expected counts normalized with DESeq2 [log₂(expected_count-deseq2+1)]. Numbers above plots are Spearman's rank rho values, which in the rages of 0.1 to 0.39, 0.4 to 0.69 and 0.7 to 1.0 are considered to be weak, moderate and strong positive correlations, respectively. The RNA-Seq data of TCGA (The Cancer Genome Atlas) thyroid carcinoma samples was analyzed through the UCSC TOIL RNAseq Recompute Data Hub on UCSC Xena (https://xena.ucsc.edu/).



Supplementary Fig. S5. Ectopic overexpression of DBT also kills MM485, 451-Lu and COLO-800 melanoma cells. (A-C) Bright field (Top) and red fluorescent images at the indicated days after transduction of the indicated cells with EF-DBT-mCherrry.